

Cosmology and Cluster Halo Scaling Relations

Pablo A. Araya-Melo^{1,2,3}, Rien van de Weygaert¹ and Bernard J.T. Jones¹

¹*Kapteyn Astronomical Institute, University of Groningen, P.O. Box 800, 9700 AV Groningen, The Netherlands*

²*Korea Institute for Advanced Study, Dongdaemon-gu, Seoul 130-722, Korea*

³*Jacobs University Bremen, Campus Ring 1, 28759 Bremen, Germany*

ABSTRACT

We explore the effects of dark matter and dark energy on the dynamical scaling properties of galaxy clusters. We investigate the cluster Faber-Jackson (FJ), Kormendy and Fundamental Plane (FP) relations between the mass, radius and velocity dispersion of cluster size halos in cosmological N -body simulations. The simulations span a wide range of cosmological parameters, representing open, flat and closed Universes.

Independently of the cosmology, we find that the simulated clusters are close to a perfect virial state and do indeed define a Fundamental Plane. The fitted parameters of the FJ, Kormendy and FP relationships do not show any significant dependence on Ω_m and/or Ω_Λ . The one outstanding effect is the influence of Ω_m on the thickness of the Fundamental Plane.

Following the time evolution of our models, we find slight changes of FJ and Kormendy parameters in high Ω_m universe, along with a slight decrease of FP fitting parameters. We also see an initial increase of the FP thickness followed by a convergence to a nearly constant value. The epoch of convergence is later for higher values of Ω_m while the thickness remains constant in the low Ω_m Λ -models. We also find a continuous increase of the FP thickness in the Standard CDM (SCDM) cosmology. There is no evidence that these differences are due to the different power spectrum slope at cluster scales.

From the point of view of the FP, there is little difference between clusters that quietly accreted their mass and those that underwent massive mergers. The principal effect of strong mergers is to change significantly the ratio of the half-mass radius r_{half} to the harmonic mean radius r_h .

Key words: Cosmology: theory – cosmological parameters – dark matter – large-scale structure of Universe – galaxies: clusters: general

1 INTRODUCTION

Recent observations of distant supernovae (Riess et al. 1998; Perlmutter et al. 1999) suggest that we are living in a flat, accelerated Universe with a low matter density. This accelerated expansion has established the possibility of a dark energy component which behaves like Einstein’s cosmological constant Λ . A positive cosmological constant resolves the apparent conflict suggested by the old age of globular cluster stars and the estimated value (Spergel et al. 2003, 2007) appears sufficient to yield a flat geometry of our Universe.

The role of Λ in the process of structure formation is not yet fully understood. Although its influence can be seen when looking at the global evolution of the Universe, its role in the dynamical evolution of cosmic structures is not clear. The most direct impact of Λ comes from its influence on the amplitude of the primordial perturbation power spectrum; there is also an influence from the change in the cosmic and dynamical time scales. The direct dynamical influence

is probably minor: we do know that in the linear regime it accounts for a mere $\sim 1/70$ th of the influence of matter perturbation (Lahav et al. 1991).

Most viable theories of cosmic structure formation involve hierarchical clustering. Small structures form first and they merge to give birth to bigger ones. The rate and history of this process is highly dependent on the amount of (dark) matter present in the Universe. In Universes with a low Ω_m , structure formation ceases at much early times than that in cosmologies with high density values.

Within this hierarchical process, clusters of galaxies are the most massive and most recently formed structures in the Universe. Their collapse time is comparable to the age of the Universe. This makes them important probes for the study of cosmic structure formation and evolution. The hierarchical clustering history from which galaxy clusters emerge involves a highly complex process of merging, accretion and virialization. In this paper we investigate in how far we can

get insight into this history on the basis of the internal properties of the clusters. This involves characteristics like their mass and mass distribution, their size and their kinetic and gravitational potential energy. In particular, we are keen to learn whether these do show any possible trace of a cosmological constant.

One particular profound manifestation of the virial state of cosmic objects is via scaling relations that connect various structural properties. Scaling relations of collapsed and virialized objects relate two or three fundamental characteristics. The first involves a quantity measuring the amount of mass M , often expressed in terms of the amount of light L emitted by the object. The second quantity involves the size of the object, while the third one quantifies its dynamical state. For a virialized halo with mass M , size R and velocity dispersion $\sigma_v = \langle v^2 \rangle^{1/2}$, the implied scaling relation is

$$\log M = 2 \log \sigma_v + \log R + \epsilon_M, \quad (1)$$

where ϵ_M is a constant that reflects the internal dynamics of the system. (ϵ_M is determined by issues such as the isotropy if the cluster velocity dispersion, its shape and any substructure).

Systems having similar values of this constant would be expected to form a two-parameter family of objects: observationally this manifests itself as the “Fundamental Plane”. Objects lying on the same plane might be expected to have similar formation histories and, conversely, the nature of the Fundamental Plane is a clue to the underlying formation mechanism.

The scaling relations are of great importance for a variety of reasons. First of all, they inform us about the dynamical state of the objects and must be a profound reflection of the galaxy formation process (Robertson et al. 2006). Also, they have turned out to be of substantial practical importance. Because they relate an intrinsic distance independent quantity like velocity dispersion to a distance dependent one like L_e , they can be used as cosmological distance indicators.

1.1 Observed relationships

1.1.1 Galaxies

Since the mid 70s, we know that the observed properties of elliptical galaxies follow scaling relations. The Faber-Jackson relation (Faber & Jackson 1976) relates the luminosity L and the velocity dispersion σ of an elliptical galaxy. The Tully-Fisher relation (Tully & Fisher 1977) is the equivalent for spiral galaxies. A different, though related, scaling is that between the effective radius r_e and the luminosity L of the galaxy. This is known as the Kormendy relation (Kormendy 1977). These two relations turned out to be manifestations of a deeper scaling relation between three fundamental characteristics, which became known as the Fundamental Plane (Djorgovski & Davis 1987; Dressler et al. 1987).

The Fundamental Plane is generally expressed as a relationship between three parameters, though there is no consensus as to which three should best be used, nor precisely how to define them. This makes detailed comparisons somewhat difficult. Some authors use the set $(\log R, \log \sigma, \log I)$, I being the luminosity in some spectral band within some radius R , while others use the set $(\log R, \log \sigma, \mu)$, μ being

the mean surface brightness within that radius. Comparisons are further complicated by the fact that there appear to be manifest residual luminosity dependences in the fits, as reported in a recent study of the SDSS by Nigoche-Netro et al. (2009).

Care is needed when interpreting these observed relationships. Observed data generally refers to luminosity rather than mass, and the radius that is used generally refers to some fiducial radius such as the half-light radius or some radius based on profile fitting. Often, the half-light radius, R_e as determined from a fit to a de Vaucouleurs profile is used.

This situation has been improved somewhat by the gravitational lensing study of Bolton et al. (2007). These authors presented a new formulation of the FP using lensing data to replace surface brightness with surface mass density. They also present an interesting alternative, which they refer to as the “Mass Plane” (MP), in which they find the dependence of $\log(R_e)$ on $\log(\sigma_{e2})$ and surface mass density Σ_{e2} within a radius $R_e/2$. Using surface mass density Σ_{e2} within a radius $R_e/2$ in place of surface brightness I_e removes one of the assumptions about the relationship between mass and light.

1.1.2 Galaxy Clusters

Much recent galaxy cluster work on the Fundamental Plane has focussed on the differences between the Fundamental Planes of the clusters as defined by their member galaxies (see for example D’Onofrio et al. (2008) and references therein).

Galaxy cluster scaling relations were discovered by Schaeffer et al. (1993) who studied a sample of 16 galaxy clusters, concluding that these systems also populate a Fundamental Plane. Adami et al. (1998) used the ESO Nearby Abell Cluster Survey (ENACS) to study the existence of a Fundamental Plane for rich galaxy clusters, finding that it is significantly different from that for elliptical galaxies. Marmo et al. (2004) using data from the WINGS cluster survey found that the difference is largely a simple shift in the relative positions of the planes.

The largely unknown relationship between mass and light frustrates a direct comparison with the results of N-Body investigations.

1.2 Numerical investigations

Later, Lanzoni et al. (2004) addressed the question using N-Body simulations for high mass halos, which are thought to host clusters of galaxies. On the basis of 13 simulated massive dark matter halos in a Λ CDM cosmology they found that the dark matter halos follow the FJ, Kormendy and FP-like relations.

In hierarchical scenarios of structure formation halos build up by subsequent merging of smaller halos into larger and larger halos. Some of these mergers involves sizeable clumps, most involves a more quiescent accretion of matter and small clumps from the surroundings. This process leaves its mark on the phase-space structure of the halos. Indeed, these dark halo streams are a major source of attention in present day studies of the formation of our Galaxy (Helmi & White 1999; Helmi 2000).

Model	Ω_m	Ω_Λ	Ω_k	Age	m_{dm}	m_{cut}	$\Delta_{vir,b}$	$\Delta_{vir,c}$
SCDM	1.0	0	0	9.31	13.23	1323	177.65	177.65
OCDM01	0.1	0	0.9	12.55	1.32	132	978.83	97.88
OCDM03	0.3	0	0.7	11.30	3.97	397	402.34	120.70
OCDM05	0.5	0	0.5	10.53	6.62	662	278.10	139.05
Λ CDM01	0.1	0.5	0.4	14.65	1.32	132	838.30	83.83
Λ CDM02	0.1	0.7	0.2	15.96	1.32	132	778.30	77.83
Λ CDMF1	0.1	0.9	0	17.85	1.32	132	715.12	71.51
Λ CDM03	0.3	0.5	0.2	12.70	3.97	397	358.21	107.46
Λ CDMF2	0.3	0.7	0	13.47	3.97	397	339.78	101.93
Λ CDMC1	0.3	0.9	-0.2	14.44	3.97	397	320.79	96.237
Λ CDMF3	0.5	0.5	0	11.61	6.62	662	252.38	126.19
Λ CDMC2	0.5	0.7	-0.2	12.17	6.62	662	241.74	120.87
Λ CDMC3	0.5	0.9	-0.4	12.84	6.62	6622	30.85	115.43

Table 1. Cosmological parameters for the runs. The first column gives the identification of the runs, and the following columns give the present matter density parameter, the density parameter associated with the cosmological constant, $\Omega_k = 1 - \Omega_m - \Omega_\Lambda$ quantifies the curvature of the Universe, the age of the Universe in Gyr since the Big Bang, the mass per particle in units of $10^{10}h^{-1}M_\odot$, the mass cut of the groups given by HOP in units of $10^{10}h^{-1}M_\odot$, the value of the (over)density needed to have virialized objects with respect to the background density, and similarly, but now with respect to the critical density.

It remains an interesting question as to whether we can find evidence for these merging events in the Fundamental Plane. González-García & van Albada (2003) look into the effects of major mergers on the Fundamental Plane and found that the Fundamental Plane does remain largely intact in the case of two merging ellipticals. However, what the effects will be of an incessant bombardment of a halo by material in its surroundings has not been studied in much detail. Given that this is a sensitive function of the cosmological scenario, we will study the influence on FP parameters and thickness in more detail.

In this paper we address the specific question as to whether we can trace an influence of cosmic parameters in the scaling relations for simulated clusters, and in particular the influence of the cosmic density parameter Ω_m and the cosmological constant Λ . We use a set of dissipationless N -body simulations involving open, flat and closed Universes. All the simulations are variants of the cold dark matter (CDM) scenario, representing different cosmologies, concerning both different values for the mass density Ω_m , for dark energy Ω_Λ and for the implied power spectrum of density perturbations and the related merging and accretion history of the clusters.

The organization of this paper is as follows. In section 2 we describe the simulations and the definitions of the various parameters we use. In section 3 we present a general description of the scaling relations which we investigate in this study before specifying the way in which we analyze them from the cluster-sized halos in our simulation. We investigate the scaling relations of galaxy clusters in different cosmologies at $z = 0$ in section 4. Section 5 addresses the evolution of the scaling relations as a function of redshift and cosmic time. We also investigate the dependence of merging and accretion on the scaling relations, which we discuss in section 6. The interpretation of our results on the Fundamental Plane within the context of the virial theorem is discussed in section 7. Conclusions are presented in section 8.

2 THE SIMULATIONS

We perform thirteen N -body simulations that follows the dynamics of $N = 256^3$ particles in a periodic box of size $L = 200h^{-1}\text{Mpc}$. The initial conditions are generated with identical phases for Fourier components of the Gaussian random field. In this way, each cosmological model contains the same morphological structures. For all models we chose the same Hubble parameter, $h = 0.7$, and the same normalization of the power spectrum, $\sigma_8 = 0.8$. The principal differences between the simulations are the values of the matter density and vacuum energy density parameters, Ω_m and Ω_Λ . By combining these parameters, we get models describing the three possible geometries of the Universe: open, flat and closed. The effect of having the same Hubble parameter and different cosmological constants translates into having different cosmic times. Table 1 lists the values of the cosmological parameters and the cosmic times at which the data is analysed.

The initial conditions are evolved up to the present time ($z = 0$) using the massive parallel tree N -body code GADGET2 (Springel 2005). The Plummer-equivalent softening was set at $\epsilon_{pl} = 15h^{-1}\text{kpc}$ in physical units from $z = 2$ to $z = 0$, while it was taken to be fixed in comoving units at higher redshifts. For each cosmological model we wrote the output of 100 snapshots, from $a_{exp} = 0.2$ ($z = 4$) to the present time, $a_{exp} = 1$ ($z = 0$), equally spaced in $\log(a)$.

2.1 Halo identification

We use the HOP algorithm (Eisenstein & Hut 1998) to extract the groups present in the simulations. HOP associates a density to every particle. In a first step, a group is defined as a collection of particles linked to a local density maximum. To make a distinction between a high density region and its surroundings, HOP uses a regrouping procedure. This procedure identifies a group as an individual object on the basis of a specific density value. For this critical value we chose the virial density value Δ_c based on the

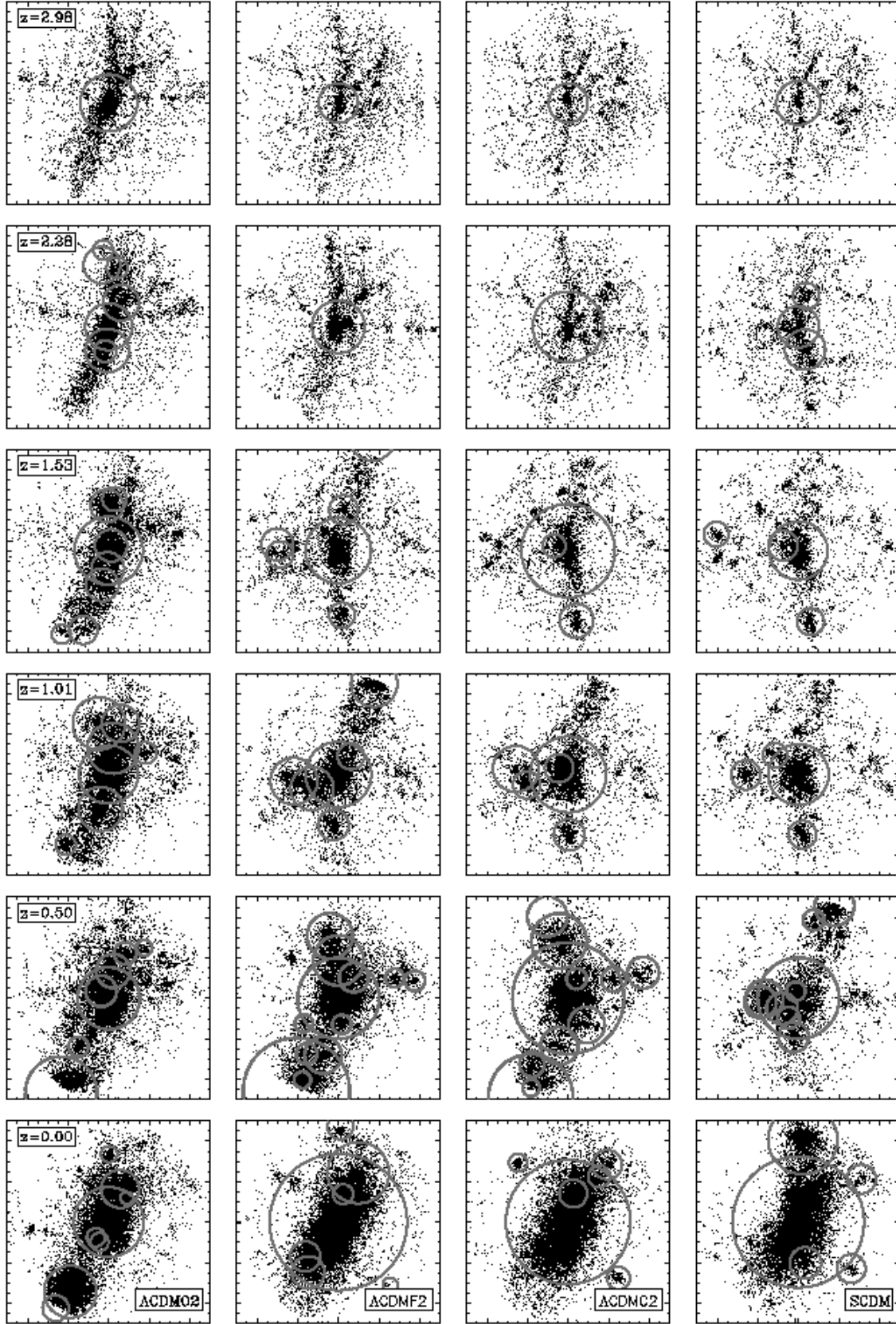


Figure 1. Cluster evolution: Ω_m influence. Evolution as a function of redshift of a single dark matter halo in different cosmological models: ACDM02, ACDMF2, ACDMC2 and SCDM. Shown is the dark matter particle distribution in a box of comoving size $5h^{-1}$ Mpc, at 6 different redshifts: $z=2.98$, $z=2.28$, $z=1.53$, $z=1.01$, $z=0.50$ and $z=0.00$. The circles correspond to halos identified by HOP, with the size of the circle being proportional to their virial radius.

Cosmic Time	SCDM	Λ CDMO2	Λ CDMF2	Λ CDMC2
2.36	1.49	4	2.71	2.21
3.26	1.01	2.92	1.98	1.60
4.06	0.74	2.35	1.56	1.24
5.07	0.50	1.83	1.19	0.93
9.31	0	0.71	0.38	0.24

Table 2. Cosmic times in Gyr and the corresponding redshift for a set of four reference cosmological models.

spherical collapse model. In order to have the proper Δ_c we numerically compute its value for each of the cosmologies. See Table 1 for the values of the virial density for each cosmology at $z = 0$. For the latter we list two values: the virial overdensity $\Delta_{vir,b}$ with respect to the background density ρ_b of the corresponding cosmology, and the related virial overdensity $\Delta_{vir,c}$ with respect to the critical density.

Note that we only consider groups containing more than 100 particles. Because the particle mass depends on the cosmological scenario, this implies a different mass cut for the halos in each of our simulations. As a result, SCDM does not have groups with masses lower than $10^{13}h^{-1}M_\odot$. We have to keep in mind this artificial constraint when considering collapse and virialization in hierarchical scenarios at high redshifts, and also when making fits to the relationships among the various cluster parameters. In cases where structure growth is still continuing vigorously at the current epoch, the collapsed halos at high redshifts will have been small: our simulations would not be able to resolve these.

2.2 Halos and Cosmology: an example

Figure 1 follows the evolution of one particular cluster halo in four different cosmologies. These are Λ CDMO2, Λ CDMF2, Λ CDMC2 and SCDM. By using the same Fourier phases to set up the initial conditions in each of the cosmologies we get a sample of corresponding halos. In each of the cosmologies the evolution of the cluster halo is shown at six different redshifts, from $z \approx 3$ onward to the present epoch $z = 0$. The panels show the mass distribution in and around the cluster, and its progenitors, in a box of comoving size $5h^{-1}$ Mpc. Circles enclose halos identified by HOP, with the circle radius proportional to the virial radius of the group (i.e. the distance from the center of mass to the outermost particle of the group). Projection effects may occasionally cause circles to appear within circles.

In all four cosmologies, the buildup of the halo clearly involves the merging of several smaller mass clumps, some of which are identified as genuine proto-halos by means of circles. Fig. 1 shows that the sequence Λ CDMO2, Λ CDMF2, Λ CDMC2 and SCDM corresponds to a sequence in which the formation of the halo shifts to later and later epochs. At all depicted redshifts, and in particular at higher redshifts, the clusters in the Λ CDMO2 cosmology have considerably more pronounced and developed mass concentration.

2.3 Halo properties

In our study, we limit ourselves to cluster-like halos. A galaxy cluster is defined as a dark matter halo with a mass $M > 10^{14}h^{-1}M_\odot$. We measure three quantities for each cluster and test their scaling relations.

Scaling relations of collapsed and virialized objects relate two or three fundamental characteristics of those objects. The first involves a quantity measuring the amount of mass, often in terms of the amount of light emitted by the object. The second quantity involves the size of the object, while the third one quantifies its dynamical state.

- **Mass:** defined as the number of particles multiplied by the mass per particle present in each group:

$$M = n_{part}m_{part}, \quad (2)$$

where n_{part} is the number of particles in the halo and m_{part} is the mass of each particle (see column m_{dm} in Table 1). The mass of the particle is different for each cosmology.

- **Surface mass density:** Alternatively, following observational practice, we use the magnitude-scale surface mass density μ for our Fundamental Plane evaluations,

$$\mu = -2.5 \log M + 5 \log r \quad (3)$$

where M and r are the mass and the radius of the halo. Combining this with a mass to light ratio it becomes a surface brightness, one of the observables of the Fundamental Plane.

- **Velocity dispersion:** computed as

$$\sigma_v^2 = \frac{2K}{n_{part}m_{part}}, \quad (4)$$

where K is the kinetic energy of the halo.

As a measure for the size of the halos, we have explored two options: the half-mass radius and the mean harmonic radius.

- **Half-mass radius:** r_{half} is the radius that encloses half of the mass of the clump. This radius is closest in definition to the half-light radius used in observational studies.

- **Mean harmonic radius:** r_h is defined as the inverse of the mean distance between all pairs of particles in the halo:

$$\frac{1}{r_h} = \frac{1}{N} \sum_{i < j} \frac{1}{|\mathbf{r}_{ij}|}, \quad N = \frac{n_{part}(n_{part} - 1)}{2}, \quad (5)$$

where \mathbf{r}_{ij} is the separation vector between the i th and the j th particle. The great virtue of this radius is that it is a good measure of the effective radius of the gravitational potential of the clump, certainly important when assessing the virial status of the clump. Also, it has the practical advantage of being independent of the definition of the cluster center. To some extent, it is also an indicator of the internal structure of the halo because it put extra weight to close pairs of particles.

Most of the results presented in this paper refer to the mean harmonic radius of the halos: this seems rather natural given that we are discussing the virial theorem (see Table

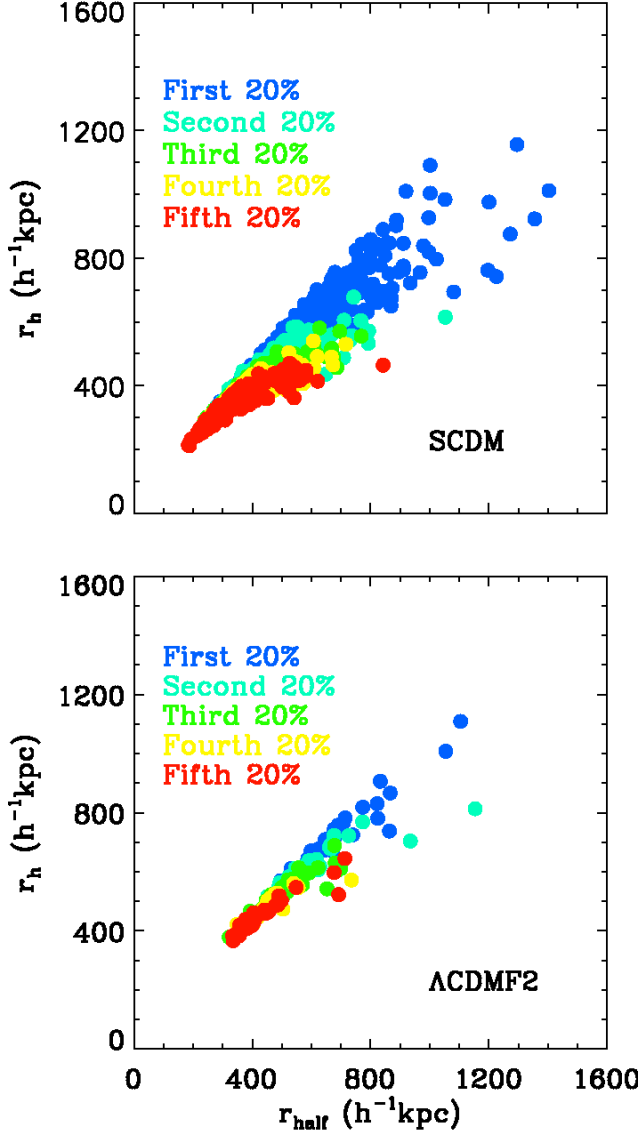


Figure 2. Comparison between the mean harmonic radius and the half-mass radius of the cluster-size halos in the SCDM (top) and Λ CDMF2 (bottom) scenarios. The colours depict different mass ranges, each colour representing a 20 percentile mass quantile.

3). We have also compared the results obtained using the half-mass radii of the halos.

In Fig. 2 we plot the mean harmonic radius versus the half-mass radius of the cluster-size halos in the SCDM and in the Λ CDMF2 models. We see that the relationship is not very tight at larger masses, and that the differences between the two radii are particularly prominent in the SCDM cosmology. We shall discuss this further in section 6. Not surprisingly, the fitted Fundamental Plane parameters depends strongly on which radius is used. Equally surprising, the Kormendy relation slope does not seem to be particularly sensitive to the choice of r_h or r_{half} (the slopes are statistically not different). This is summarised in Table 6.

3 SCALING RELATIONS

For the samples of cluster-sized halos in our simulations we will be assessing three specific scaling relations: the Faber-Jackson relation, the Kormendy relation and the Fundamental Plane.

From observations of elliptical galaxies we have learned that there are tight scaling relations between a few of their fundamental structural properties (see e.g. Binney & Merrifield (1998)). These properties are the total luminosity L of a galaxy - or its surface brightness μ - its characteristic size R_e and its velocity dispersion σ_v .

3.1 Faber-Jackson and Kormendy Relations

The first scaling relation is the Faber-Jackson relation (Faber & Jackson 1976) between the luminosity L of the galaxy and its velocity dispersion σ_v ,

$$L \propto \sigma_v^\beta, \quad (6)$$

where the index $\beta \sim 4$. A similar relation, known as the Tully-Fisher relation (Tully & Fisher 1977), holds for HI disks of spiral galaxies. According to this relation, the galaxies' rotation velocity is tightly correlated with the absolute magnitude of the galaxy.

Another relation was established by Kormendy (1977). He found that there is a strong, not entirely unexpected, correlation between the luminosity L and effective radius R_e of the elliptical galaxies:

$$L \propto R_e^\alpha, \quad (7)$$

where the index $\alpha \sim 1.5$.

3.2 Galaxy Fundamental Plane

Both the FJ and Kormendy relations relate two structural characteristics and should be seen as projections of a more fundamental and tight relation between all three structural quantities: the *Fundamental Plane* (FP). The Fundamental Plane of elliptical galaxies was first formulated by Djorgovski & Davis (1987) and Dressler et al. (1987). When we take the three-dimensional space defined by the effective radius R_e of the galaxy, its surface brightness I_e (with total luminosity $L \propto I_e R_e^2$) and velocity dispersion σ_v , we find that they do not fill space homogeneously but instead define a thin plane.

In logarithmic quantities, this plane may be parameterized as

$$\log R_e = \gamma \log I_e + \delta \log \sigma_v + C_{fp} \quad (8)$$

For example, Jørgensen et al. (1996) found that a reasonable fit to the Fundamental Plane is given by

$$\log R_e = -0.82 \log I_e + 1.24 \log \sigma_v + C_{fp} \quad (9)$$

While nearly all galaxies, ranging from giant ellipticals to compact dwarf ellipticals, appear to lie on the FP (also see e.g. Jørgensen et al. 1995; Bernardi et al. 2003; Cappellari et al. 2006; Bolton et al. 2007) it is interesting to note that diffuse dwarf ellipticals do not (Kormendy 1987): they seem to be fundamentally different objects.

The observed Fundamental Plane not only provides information on the dynamical state of the object but also on

Model	Ω_m	Ω_Λ	$r_h \propto M^a$		$\sigma \propto M^b$		$\log r_h = c\mu + d \log \sigma + C_{fp}$					
			a	S_K	b	S_{FJ}	c	σ_c (10^{-2})	d	σ_d (10^{-2})	S	w_{fp} (10^{-3})
SCDM	1	0	0.38	0.06	0.33	0.03	0.37	0.31	1.78	1.14	0.03	14.03
OCDM01	0.1	0	0.34	0.05	0.37	0.03	0.35	1.73	1.60	8.27	0.02	8.57
OCDM03	0.3	0	0.36	0.05	0.33	0.03	0.38	1.10	1.76	4.13	0.03	13.41
OCDM05	0.5	0	0.37	0.05	0.33	0.03	0.37	0.53	1.79	2.01	0.03	12.24
Λ CDMO1	0.1	0.5	0.35	0.05	0.38	0.03	0.37	1.55	1.60	7.56	0.02	7.51
Λ CDMO2	0.1	0.7	0.38	0.05	0.35	0.03	0.38	1.90	1.66	8.84	0.02	8.44
Λ CDMF1	0.1	0.9	0.35	0.05	0.36	0.03	0.38	1.64	1.69	7.93	0.01	6.97
Λ CDMO3	0.3	0.5	0.36	0.05	0.34	0.03	0.41	1.03	1.86	3.88	0.03	11.43
Λ CDMF2	0.3	0.7	0.36	0.05	0.33	0.03	0.41	1.11	1.88	4.01	0.02	11.23
Λ CDMC1	0.3	0.9	0.34	0.05	0.34	0.03	0.42	1.19	1.92	4.33	0.03	11.09
Λ CDMF3	0.5	0.5	0.35	0.05	0.34	0.03	0.38	0.56	1.81	2.10	0.03	11.75
Λ CDMC2	0.5	0.7	0.35	0.05	0.34	0.03	0.38	0.57	1.82	2.14	0.03	11.66
Λ CDMC3	0.5	0.9	0.34	0.05	0.34	0.03	0.39	0.61	1.83	2.31	0.03	12.24

Table 3. Parameters of the scaling relations derived for the galaxy clusters in each of the simulated cosmological simulations. r_h is the mean harmonic radius of the cluster. a is the scaling parameter for the Kormendy relation, b is the scaling parameter for the Faber-Jackson relation and c and d are the scaling parameters for the Fundamental Plane. σ is the standard error in each of the scaling relation parameters, S is the corresponding standard error/significance of the fit.

the evolution of its stellar content and, by implication, about its formation. For a virialized object with effective radius R_e and mass-to-light ratio M/L the FP relation will have the form

$$\log R_e = -\log I_e + 2 \log \sigma_v - \log(M/L) + C_s, \quad (10)$$

in which $I_e = L/4\pi R_e^2$ is the mean surface brightness and C_s a constant dependent on the structure of the object.

The observed parameter values for elliptical galaxy Fundamental Plane (see Eqn. 9) are different from what might be expected for a plane that results simply from virialization and constant mass-to-light ratio. One explanation for this difference is that galaxies may be structurally equivalent while having a mass-dependent M/L ratio. That would imply a formation process involving a tight fine tuning of M/L . Nevertheless, pursuing this view, the parameters inferred by Jørgensen et al. (1996) (Eqn. 9) would imply a mass-to-light ratio dependence on mass:

$$(M/L) \propto M^{0.25}, \quad (11)$$

using $M \propto \sigma_v^2 R_e$ and $L \propto I_e R_e^2$ (see e.g. Faber 1987). Recent semi-analytical modelling of galaxy formation suggest a more complex relation between the mass-to-light ratio and luminosity, involving a minimum M/L for galaxies with $M \approx 10^{11} - 10^{12} h^{-1} M_\odot$. In the absence of any mass-to-light dependency, the discrepancy between the planes would have to be due to variations in the structure parameters of the galaxies.

There is an intrinsic scatter of the FP that has been found for elliptical galaxies: this has not been completely explained and may be a manifestation of the formation process.

A slightly different approach is used in the gravitational lensing study of Bolton et al. (2007). These authors presented a new formulation of the FP using lensing data to replace surface brightness with surface mass density, arriving at the relationship of the form

$$\log R_e = \gamma \log I_e + \delta \log \sigma_{e2} + C_{fp}, \quad (12)$$

where σ_{e2} is the velocity dispersion within half of the effective radius R_e , and

$$\gamma = -0.78 \pm 0.13, \quad \delta = 1.50 \pm 0.32, \quad C_{fp} = 3.9 \pm 1.7. \quad (13)$$

Furthermore they suggest that the scatter about the Fundamental Plane, derived from their data, correlates with their derived mass-to-light ratio for the galaxies in their sample. The evidence is not strong though it is suggestive.

They also present an interesting alternative, which they refer to as the “Mass Plane” (MP), in which they find the dependence of $\log(R_e)$ on $\log(\sigma_{e2})$ and surface mass density Σ_{e2} within a radius $R_e/2$:

$$\log R_e = \gamma_m \log \Sigma_{e2} + \delta_m \log \sigma_{e2} + C_{fp,m} \quad (14)$$

with

$$\gamma_m = -1.16 \pm 0.09, \quad \delta_m = 1.77 \pm 0.14, \quad C_{fp} = 7.8 \pm 1.0. \quad (15)$$

Using surface mass density Σ_{e2} within a radius $R_e/2$ in place of surface brightness I_e removes one of the assumptions about the relationship between mass and light.

3.3 Cluster Fundamental Plane

If clusters were fully virialized objects with the same internal dynamics, they would necessarily lie on a universal Fundamental Plane in the Mass-velocity-radius space. This was first addressed by Schaeffer et al. (1993), who, using sample of 29 Abell clusters, discovered a FP relation in light-velocity-radius space : $L \propto R_e^{0.89} \sigma_v^{1.28}$. This is equivalent to the relationship

$$\log R_e = -0.90 \log I_e + 1.15 \log \sigma_v + C_{fp}, \quad (16)$$

in which I_e is a measure of the mean surface brightness of the cluster. The corresponding FJ relation is $L \propto R_e^{1.87}$ and

the Kormendy relation is $L \propto R_e^{1.34}$. Similar numbers were inferred by Lanzoni et al. (2004), $L \propto R_e^{0.90} \sigma_v^{1.31}$.

In a project designed to test this further, Adami et al. (1998) found a FP relation for a sample of ENACS Clusters, though their fitted parameters were markedly different: $L \propto R^{1.19 \pm 0.14} \sigma^{0.91 \pm 0.16}$. This is equivalent to the relationship

$$\log R_e = -(1.23 \pm 0.20) \log I_e + (1.12 \pm 0.11) \log \sigma_v + C_{fp}, \quad (17)$$

in which I_e is the mean surface brightness of the cluster. Note that there are considerable systematic uncertainties in these values which are not reflected in the quoted error bars: these arise out of the profile fitting to the cluster. The above fit to the data is based on fitting a King profile, (this gave the best fit to the data).

In studies of simulated dark matter dominated galaxy clusters, we can study scaling relations that are similar to those inferred from observable quantities. To infer these relations we base ourselves on the mass M of the object. If the selected objects have the same average density, we would expect an equivalent Kormendy relation given by

$$M \propto R_e^3. \quad (18)$$

Any difference in slope should be ascribed to a dependence of mean density $\langle \rho(R_e) \rangle$ on the size R_e of the object. The equivalent Fundamental Plane relation will be that of Eqn. 1, while the Faber-Jackson relation would then be

$$M \propto \sigma_v^3. \quad (19)$$

Note that this is based on the assumption of constant mean density ρ of the selected objects, in line with HOP overdensity criterion (see sec. 2.1).

Lanzoni et al. (2004) analyzed the N-Body cluster scaling relations on the basis of a sample of 13 massive dark matter halos identified in a high resolution Λ CDM N -body simulations. They were able to confirm the existence of FP relations for the simulation dark matter clusters and also found that these have a slope that was significantly different from the galaxy FP slope,

$$\log R_e = (0.44 \pm 0.02) \mu + (1.92 \pm 0.12) \log \sigma_v + C_{fp}, \quad (20)$$

with μ the surface mass density (Eqn. 3). The difference in FP parameters between the dark matter halos and those inferred for the observed cluster sample (see above, Eqn. 17) formed a key aspect of their study. They suggest a mass dependent cluster M/L ratio

$$(M/L) \propto M^{0.8}. \quad (21)$$

would be able to explain the observed cluster Fundamental Plane. Interestingly, this is markedly different from that inferred for early type galaxies. Of course there is no obvious reason why the Fundamental Plane for galaxies should have any bearing on the Fundamental Plane for clusters. Indeed, as we shall see for the ENACS sample, its FP parameters values seem to be irreconcilable with the virial theorem.

3.4 Determination of Scaling Relations

For the sample of N cluster-sized halos in each simulation we study the scaling relations between their size r , mass M - or equivalent surface mass density μ - and velocity dispersion σ (note that N is in general different for each cosmology).

Given the inferred mass M (Eqn. 2), velocity dispersion σ_v (Eqn. 4) and the mean harmonic radius r_h (Eqn. 5) of the cluster halos, we find the scaling relation parameters by linear fitting of the relations.

Sample selection effects play a complex role in the analysis of real data samples (La Barbera et al. (2003)). Fortunately the issue is far simpler when analysing clusters found in N-Body models where the only selection criterion is a mass cut-off imposed by the cluster finding algorithm. We deal with that simply by making the Mass of the cluster the independent variable in all fits where relevant: this eliminates biases introduced through this object selection.

3.4.1 Kormendy Relation

For the Kormendy relation we fit

$$\log r = a \log M + C_a. \quad (22)$$

to the N data points $(\log r_i, \log M_i)$ of the halo sample. The significance S_K is computed from the N residuals:

$$S_K = \sqrt{\frac{1}{(N-1)} \sum_i^N (\log r_i - a \log M_i - C_a)^2} \quad (23)$$

3.4.2 Faber-Jackson Relation

Along the same line, the Faber-Jackson relation is determined on the basis of the fit

$$\log \sigma_v = b \log M + C_b, \quad (24)$$

whose significance S_{FJ} is calculated as follows:

$$S_{FJ} = \sqrt{\frac{1}{(N-1)} \sum_i^N (\log \sigma_{v,i} - b \log M_i - C_b)^2} \quad (25)$$

3.4.3 Fundamental Plane

Instead of fitting the Fundamental Plane in the form of Eqn. 1, we do it in the way suggested by the observational work, i.e., using the surface mass density μ and velocity dispersion σ_v as free parameters from which we determine a model for the radius,

$$\log r = c \mu + d \log \sigma_v + C_{fp}. \quad (26)$$

In this, μ is the magnitude-scale surface mass density (Eqn. 3). Although there are errors in determining both σ_v and μ , they are very small when compared with the dispersion about the Fundamental Plane. By fitting the parameters c and d this way we solve problems regarding biases in the mass (luminosity) selection.

The significance S_{fp} of the Fundamental Plane fits derived from the sample of N simulation cluster halos is computed according to:

$$S_{fp} = \sqrt{\frac{1}{(N-2)} \sum_i^N (\log r_i - c \mu_i - d \log \sigma_v - C_{fp})^2}. \quad (27)$$

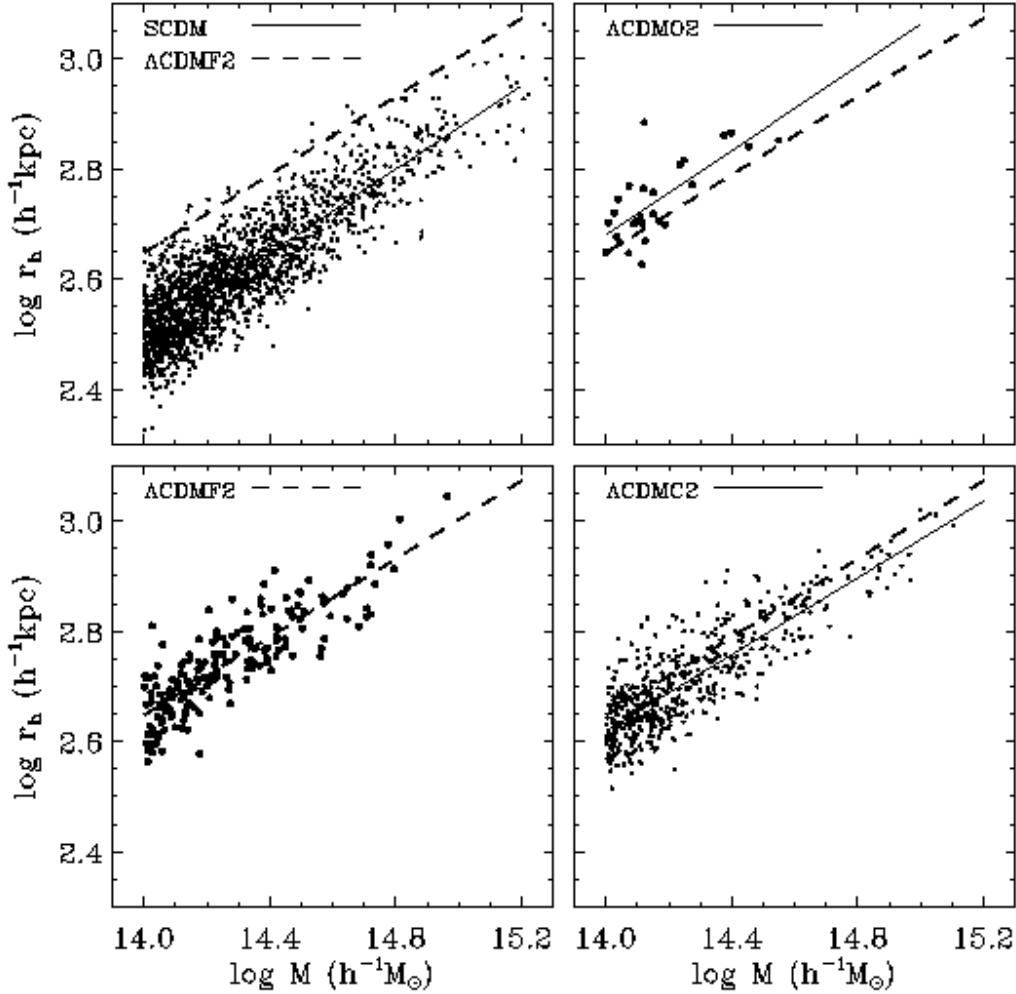


Figure 3. Kormendy Relation. Each panel plots the relation between mean harmonic radius r_h and mass M of the cluster-sized dark halos in the simulations corresponding to one particular cosmology. Going from top left to bottom right these are: SCDM, Λ CDMO2, Λ CDMF2 and Λ CDMC2. In each of the panels we have superimposed the fitted Kormendy relation for the corresponding model and for Λ CDMF2 as comparison.

The thickness w_{fp} of the Fundamental Plane is estimated on the basis of the perpendicular distances of the cluster halos to the fitted plane:

$$w_{fp} = \sqrt{\frac{\sum D_{\perp}^2}{N}}, \quad (28)$$

where N is the number of cluster halos in the sample and D_{\perp} is the perpendicular distance of a point to a plane

$$D_{\perp} = \frac{c\mu + d \log \sigma_v + C_{fp} - \log r_h}{(c^2 + d^2 + 1)^{1/2}}. \quad (29)$$

4 SCALING RELATIONS IN DIFFERENT COSMOLOGIES: $z=0$

We first investigate the scaling relations of the cluster dark matter halos in our cosmological models at the current epoch, $z = 0$, and look for possible systematic differences

between the parameter values and FP thickness as a function of the cosmology. The parameters of the resulting linear fits, to be discussed in the following subsections, are listed in Table 3.

4.1 Kormendy Relation

Fig. 3 shows the relation between the mean harmonic radius r_h of each cluster halo and their mass M . Each of the four panels depicts the relation for the halos in one particular simulated cosmology. The top left panel shows the SCDM cosmology, the top right one the Λ CDMO2 model, the bottom left one the Λ CDMF2 model and the bottom right one the Λ CDMC2 model.

In each cosmology there is a strong and systematic almost linear relation between $\log M$ and $\log r_h$: the Kormendy relation appears to be a good description for all situations. A visual comparison between SCDM relation (top left panel), the Λ CDMO2 relation (top right panel) and the

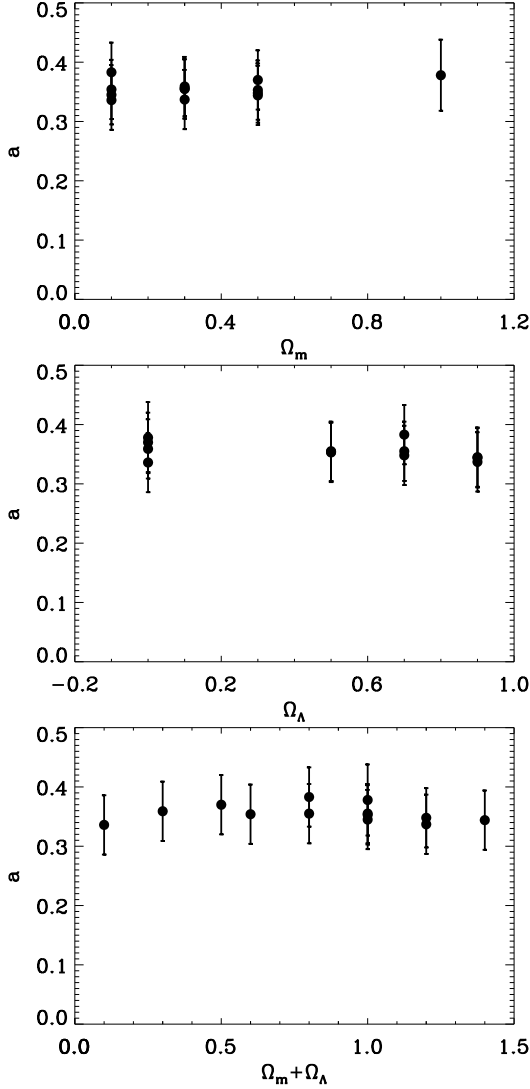


Figure 4. Inferred parameter a for the Kormendy relation (Eqn. 22) as a function of Ω_m (top panel), Ω_Λ (central panel) and $\Omega_m + \Omega_\Lambda$ (bottom panel). The bars represent the 1σ uncertainty range around the estimated parameter.

Λ CDMF2 relation (bottom left panel) shows that clusters of comparable mass have a larger size in the low Ω_m cosmology than in the ones with a higher density value. In other words, clusters are more compact in the SCDM cosmology. Not unexpectedly we find objects of a higher density in higher Ω_m models.

When fitting the plotted point distributions, we infer the parameter values listed in Table 3. In each of the panels in Fig. 3 we plotted the linear fits for all of the four depicted cosmologies. We find similar slopes for all cosmologies, in the order of $a \sim 0.36 - 0.38$. This seems to imply that the mean density $\langle \rho(r_h) \rangle \propto M^{-0.1}$: more massive halos have a slightly lower average density (see also Lanzoni et al. (2004)). To investigate the dependence of the Kormendy parameter a on the cosmology in Fig. 4 we have plotted the slope a as a function of the average mass density parameter Ω_m (top panel), as a function of the cosmological constant Ω_Λ (central panel) and as a function of the cosmic curvature,

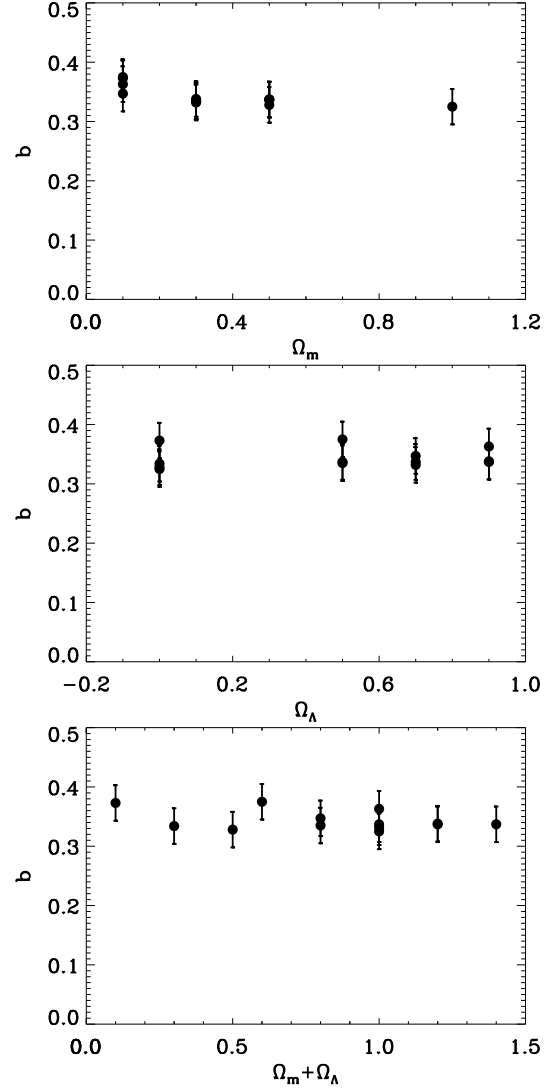


Figure 5. Inferred scaling parameter b for the FJ relation as a function of three different parameters: Ω_m (top panel), Ω_Λ (central panel) and $\Omega_m + \Omega_\Lambda$ (bottom panel). The bars represent the 1σ uncertainty range around the estimated parameter.

in terms of $\Omega_{total} = \Omega_m + \Omega_\Lambda$ (lower panel). There is no evidence for any systematic trends of the Kormendy parameter as a function of cosmology. No evidence for an influence of either cosmic density Ω_m and Ω_Λ on the internal structure of the halos could be detected.

4.2 Faber-Jackson Relation

Fig. 6 shows the Faber-Jackson relation: the relation between the mass M and the velocity dispersion σ_v of the cluster halos. Like in Fig. 3, each of the four panels corresponds to one particular simulated cosmology: SCDM (top left panel), Λ CDMO2 (top right panel), Λ CDMF2 (bottom left panel) and Λ CDMC2 (bottom right panel).

For comparison, in each of the panels we show the line of the Λ CDMF2 model corresponding to the linear fit of this relation in each of the depicted cosmologies. The $M - \sigma_v$ relation is clearly well fitted by the Faber-Jackson like relation.

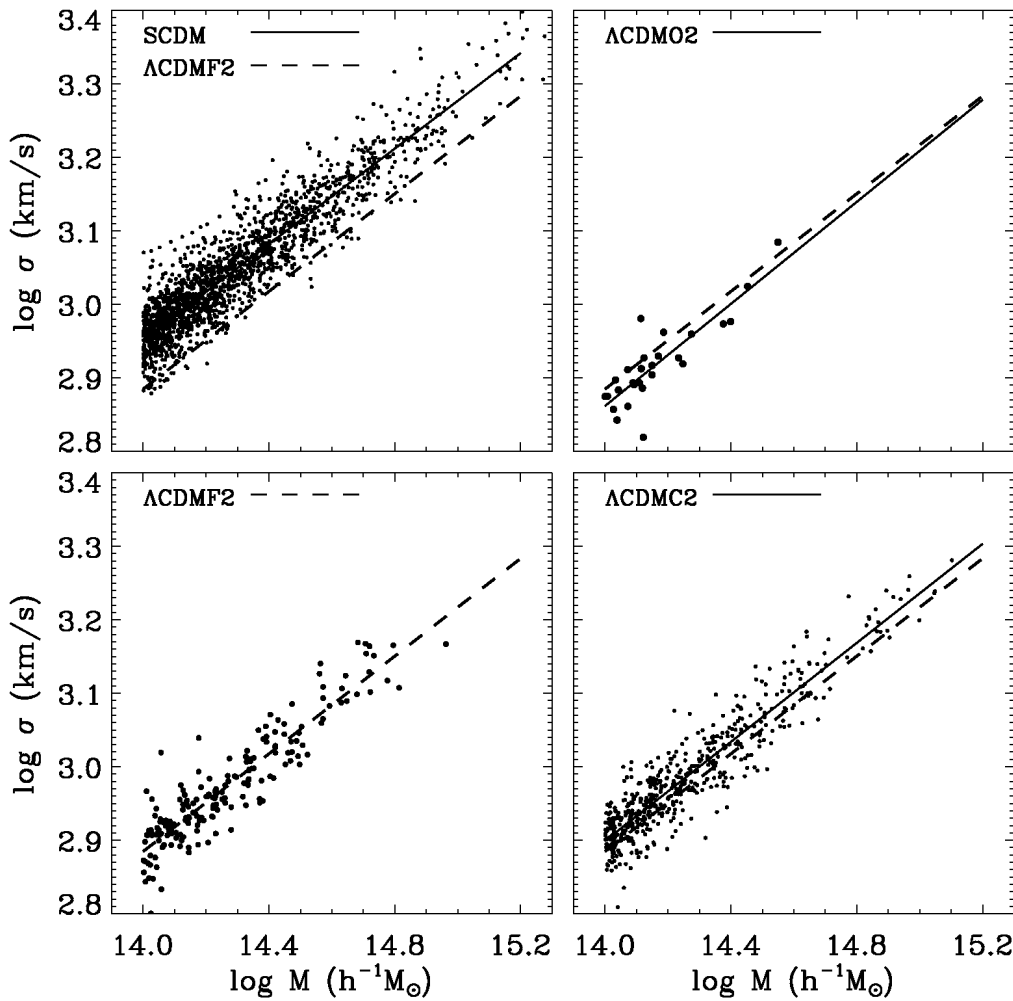


Figure 6. Faber-Jackson relation. Each panel plots the relation between the velocity dispersion σ_v and the mass M of the cluster-sized dark halos in the simulations corresponding to one particular cosmology. Going from top left to bottom right these are: SCDM, Λ CDMO2, Λ CDMF2 and Λ CDMC2. In each of the panels we have superimposed the fitted Faber-Jackson relation for the corresponding model and for Λ CDMF2 for comparison.

It is considerably tighter than the equivalent Kormendy relation.

It is also interesting to note that, as with the Kormendy relation, we do not find any significant dependence of the FJ relation on the underlying cosmology: the slope b in all cases is in the order of $b \sim 0.35$ (see Table 3). We also did not find any dependence on Ω_Λ or Ω_{total} (see Fig. 5).

Although the difference between the inferred value of $b \sim 0.35$ in most cosmologies and the value of $b = 0.33$ expected for virialized perfectly homologous systems (see Eqn. 19) is not really significant, the consistent and systematic value $b > 0.33$ might be suggestive for a weakly homologous population along the lines described in e.g. Bertin et al. (2002).

4.3 Fundamental Plane

The Kormendy relation and the Faber-Jackson relation are two dimensional projections of an intrinsically three dimen-

sional relation between mass M , size r and velocity dispersion σ_v of the halos. By implication, the spread of the Fundamental Plane relation should be less than that of each of the two previous relations.

The Fundamental Plane obtained for the same cosmologies as shown in Fig. 3 and 6 (SCDM, Λ CDMO2, Λ CDMF2 and Λ CDMC2) is illustrated in Fig. 7. In each of the frames we have plotted the harmonic radius r_h of the halos against the quantity $Y = c\mu + d \log \sigma_v + C_{FP}$ on a log-log plot. The parameters c and d in the latter quantity, Y , combining the surface mass density μ and the velocity dispersion σ_v of each halo, are the best fit FP parameters for the corresponding cosmology (see Table 3).

The galaxy clusters in each cosmology do indeed seem to populate a tightly defined plane. The point clouds in each of the frames confirm our expectation that they should have a much lower scatter around the plane than in the case of the Kormendy and Faber-Jackson relation (see Table 3).

From Table 3 we find a surprising level of consistency

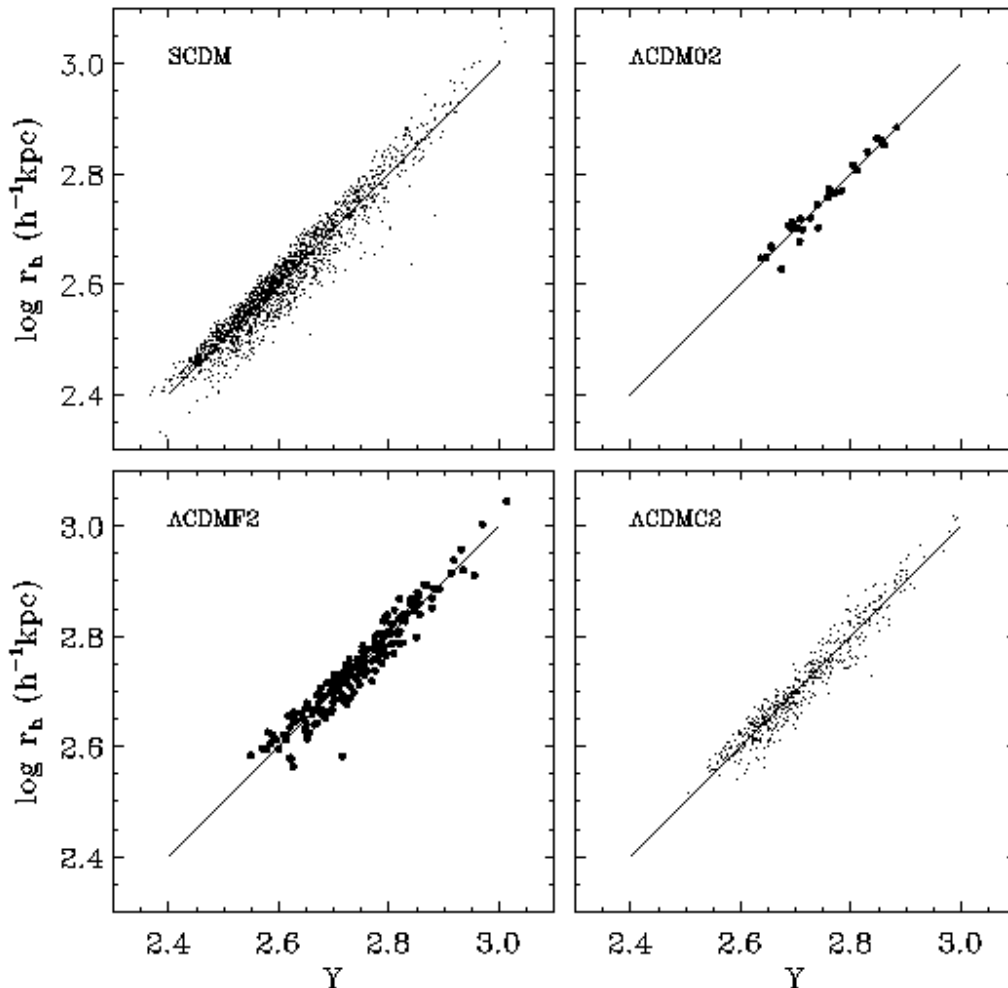


Figure 7. Fundamental Plane. Each panel plots the relation between harmonic radius r_h and the quantity $Y = c\mu + d \log \sigma$. Combining the surface mass density μ and velocity dispersion σ_v , the scaling parameters c and d are the ones inferred from the FP fitting procedure. Top left panel: the relation between harmonic halo radius r_h and Y for the cluster halo sample in the SCDM simulation. Top right panel: for the halos in the Λ CDMO2 simulation. Bottom left panel: for the halos in the Λ CDMF2 simulation. Bottom right panel: for the halos in the Λ CDMC2. The superimposed lines in each panel represent the relation for the fitted Fundamental Plane for the corresponding cosmology. Note that, by definition, each of these fitted lines should have slope unity.

between the Fundamental Planes in each of the cosmologies. We find that the inferred parameters are close to the one theoretically expected for perfectly homologous virialized clusters halos. The inferred scaling parameter c for the surface density μ hovers around $0.38 - 0.42$, close to the theoretical value $c \approx 0.4$ ($M \propto r_h \sigma_v^2$). The difference is somewhat larger for the parameter d , implying that the velocity dispersion scaling has a difference of $\sim 0.15 - 0.25$ from the theoretical value of 2.

As can be seen in both Table 3 and Fig. 7, there is hardly any variation between the FP relations in the different cosmologies: they almost all coincide. This is certainly true concerning the FP parameters c and d . The two top panels of Fig. 9 do confirm the impression that there is no systematic difference as a function of Ω_m and/or Ω_Λ . This in itself is a strong argument against differences in the scaling

relations parameters being due to a partial or incomplete level of virialization, as was claimed by Adami et al. (1998).

One possible difference between the Fundamental Plane in different cosmologies may concern its thickness w_{fp} . Inspection of Fig. 7 does suggest a marginally lower thickness of the FP for Universes with a low $\Omega_m \sim 0.1$. There is no detectable effect at all with respect to the cosmological constant Ω_Λ . We might understand a dependence on Ω_m , or cosmological constant Ω_Λ , in terms of the ongoing evolution of the cluster population. In low Ω_m Universes - and in high Ω_Λ universes all clusters formed at high redshift and have since had ample time to reach full virialization and hence tighten the corresponding Fundamental Plane. In high Ω_m Universes, clusters would still undergo a substantial levels of merging and accretion, both of which may affect the virial state of the cluster. Our computer experiments do not seem

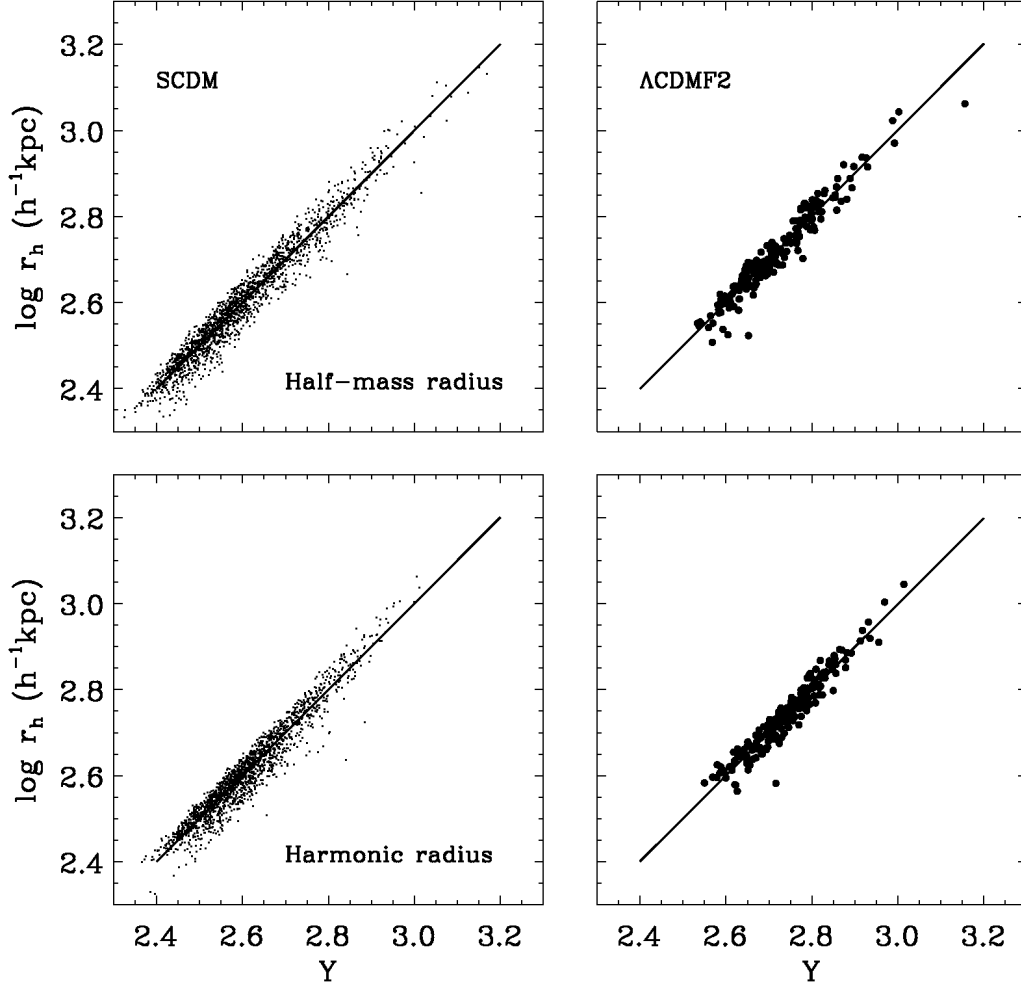


Figure 8. Fundamental Plane relation of dark halos in the SCDM (left) and Λ CDMF2 (right) cosmology, using the half-mass radius r_{half} (top row) and the harmonic radius r_h (bottom row). Plotted are mass M versus the FP quantity $Y = c\mu + d\log\sigma$, with c and d the scaling parameters inferred from the (linear) fitting procedure. The lines represents the best fit FP relations.

Model	Ω_m	Ω_Λ	Radius	$r \propto M^a$		$\log r_h = c\mu + d\log\sigma + C_{fp}$		
				a	\mathcal{S}_K	c	d	\mathcal{S}_{fp}
SCDM	1	0	Half-mass	0.39	0.09	0.29	1.60	0.03
			Harmonic	0.38	0.06	0.37	1.78	0.03
Λ CDMF2	0.1	0.7	Half-mass	0.36	0.08	0.30	1.53	0.02
			Harmonic	0.38	0.05	0.38	1.66	0.02
Λ CDMF2	0.3	0.7	Half-mass	0.35	0.07	0.31	1.66	0.03
			Harmonic	0.36	0.05	0.41	1.88	0.02
Λ CDMC3	0.5	0.9	Half-mass	0.35	0.08	0.30	1.63	0.03
			Harmonic	0.35	0.05	0.38	1.82	0.03

Table 4. Scaling relation parameters and radius definition: inferred Kormendy relation parameter a and Fundamental Plane parameters c and d , based on the use of half mass radius r_{half} and harmonic radius r_h . For four different cosmologies – SCDM, Λ CDMF2, Λ CDMF2 and Λ CDMC3 – the scaling parameters and the corresponding goodness-of-fit \mathcal{S} (see Eqn. 23 and Eqn. 27) are given for r_{half} (top row) and r_h (bottom row).

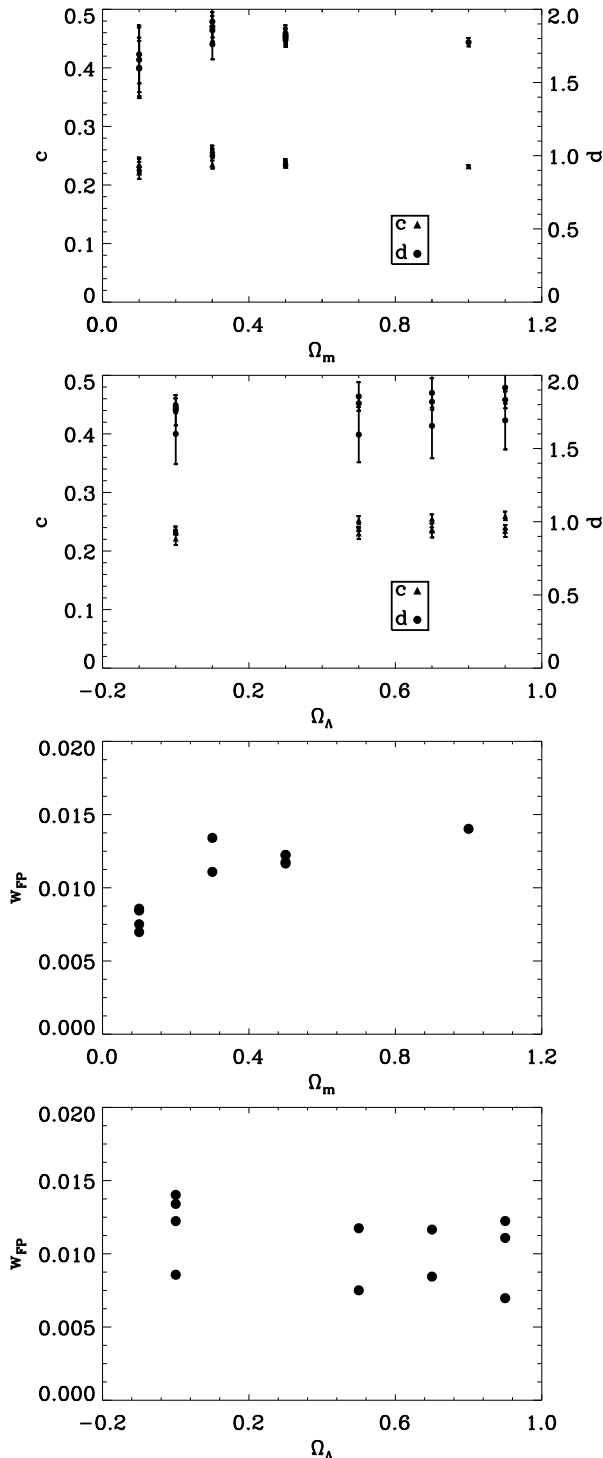


Figure 9. Top panel: Fundamental Plane parameters c (left axis, solid circles) and d (righthand axis, solid triangles) as a function of Ω_m . Second panel: Fundamental Plane parameters c (left axis, solid circles) and d (righthand axis, solid triangles) as a function of Ω_Λ . Third panel: thickness w_{FP} of the Fundamental Plane, i.e. rms scatter of the FP relation as a function of Ω_m . Bottom panel: thickness w_{FP} of the Fundamental Plane, i.e. rms scatter of the FP relation as a function of Ω_Λ .

to find any strong and significant dependence on overall cosmology.

We investigate the relationship between the FP thickness and the dynamical state of the cluster in more detail in section 6.

Finally, we can try to relate the Fundamental Plane (μ , r_h , σ_v) of our simulated cluster samples to the observationally measured (L , R_e , σ_v) plane, e.g. $L \propto R^{1.19} \sigma^{0.91}$ found for the ENACS survey.. We can ask whether the difference can be ascribed solely to a mass dependent mass-to-light ratio M/L .

4.4 Scaling Relations for alternative Radius Definition

Apart from the mean harmonic radius that we have used as a measure of halo size in the previous sections, we have also assessed the viability of the scaling relations in case of alternative size definitions. In Table 4.3 we list the resulting parameters for the Kormendy relation and the Fundamental Plane in the case of using the half-mass radius r_{half} .

The parameters for the Kormendy relation hardly differ from the ones inferred on the basis of the mean harmonic radius. However, the inferred Fundamental Plane parameters do differ significantly from the ones inferred above on the basis of the mean harmonic radius. The change in scaling parameter values may be ascribed to the use of quantities that probe different aspect of the structure and dynamics of the halos. In an extreme situation, this might have disrupted the scaling relations. Our finding shows that the Kormendy relation still holds, while the FP relation still holds but in a slightly different guise. It may be an indication for our contention that halos do not form a perfectly a homologous population. Size measures sensitive to different aspects of the halos' internal mass distribution may then result in somewhat different scaling properties. In this respect, we agree with the conclusions of Adami et al. (1998) and Lanzoni et al. (2004).

See section 6 and 7 for a discussion of the relationship between the radii r_{half} and r_h , where we show that it is a consequence of the cluster building process.

5 EVOLUTION OF SCALING RELATIONS

In the previous sections we have extensively studied the scaling relations at the current cosmic epoch $z = 0$. We have also noted that there are differences between the scaling relation parameters that we find in our simulations and those for perfect virialized and homologous systems. This makes it interesting to trace the evolution of the different scaling relations.

In this section we investigate the evolution of the scaling relations as a function of redshift and as a function of cosmic look-back time. While observers usually think in terms of redshift, it is important to appreciate that a given redshift corresponds to an entirely different dynamical epoch in different cosmologies. Given the same Hubble parameter, the age of the Universe is a sensitive function of the cosmic density parameter Ω_m and even more so of the cosmological constant. As for the latter, we have to realize that the change in cosmic time as a function of the cosmological constant is

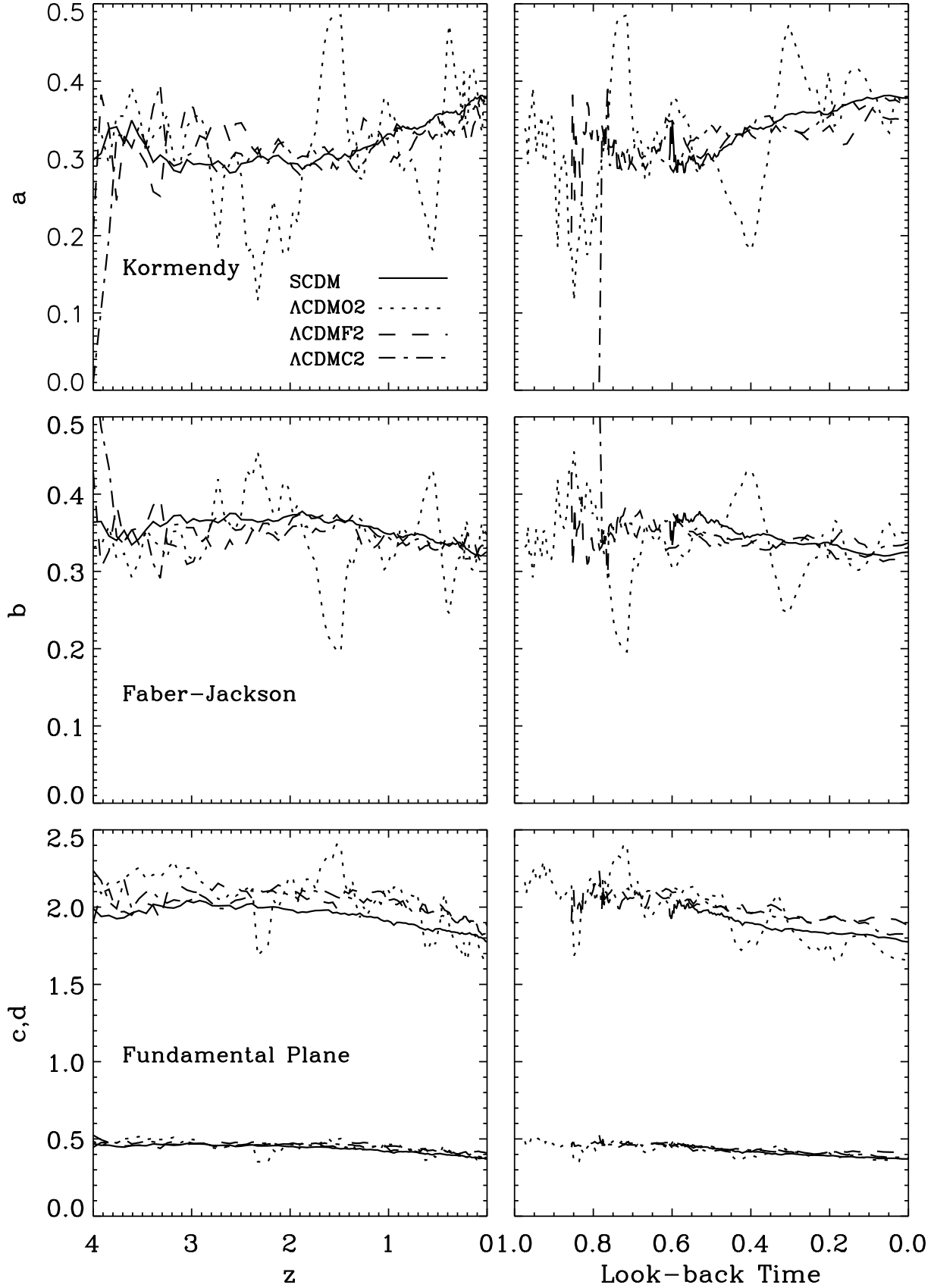


Figure 10. Evolution of the fitted scaling relation parameters as a function of redshift (left column) and as a function of cosmic look-back time (right column). Top: Kormendy parameter a . Center: Faber-Jackson parameter b . Bottom: FP parameters c and d .

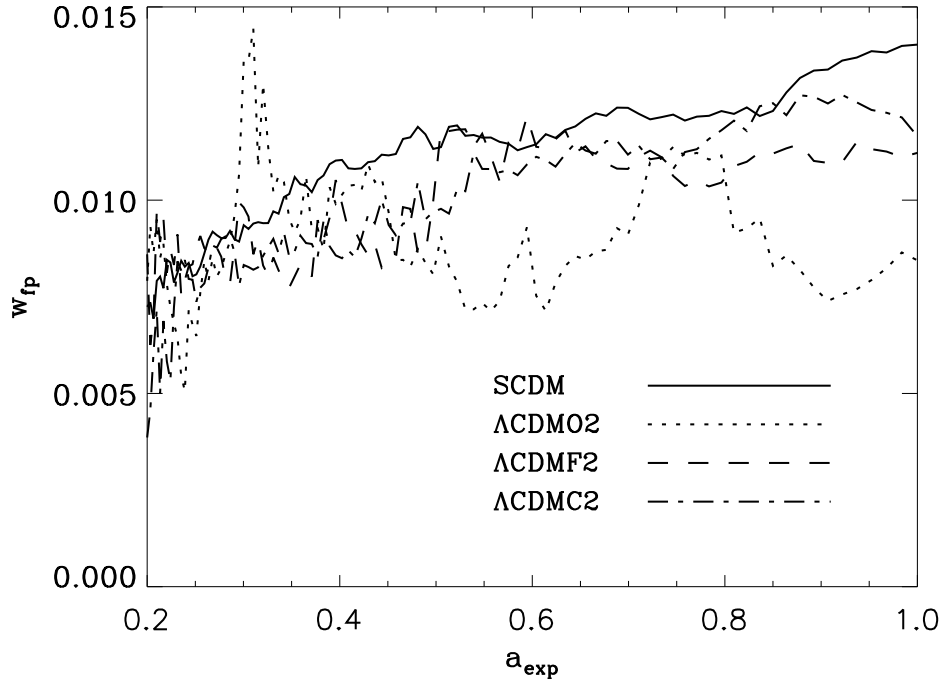


Figure 11. Evolution of the thickness of the Fundamental Plane for four different cosmologies. Note the almost consistently tighter FP for the low Ω_m Universe and the modest increase of FP thickness in the other cosmologies. The SCDM, Λ CDMF2 and Λ CDMC2 models are very similar in their behaviour. The more erratic behaviour of the Λ CDMO2 may in part be due to the smaller sample size

the most important influence of Λ . To give an appreciation of the differences in cosmic time for a given redshift in the different cosmologies, we refer to Table 2.

We have probed the scaling relations over a range of redshifts from $z = 4$ to $z = 0$ and over a range of cosmic look-back time going from 1 to 10 Gyr. The evolution of the fitted scaling parameters as a function of redshift is shown in the left column of Fig. 10. The corresponding evolution as a function of cosmic look-back time can be found in the right hand column. The Kormendy parameter a is shown in the top panels, the Faber-Jackson parameter b in the center panels and the FP parameters c and d in the bottom panels. Each different cosmology is represented by a different linestyle, listed in the insert at the top left hand frame.

5.1 Evolution of the Kormendy relation

For all cosmologies the evolution of the Kormendy relation is marginal at best. In the case of the low Ω_m Λ CDMO2 cosmology we can not discern any significant change of the parameter a , (this may in part be due to the large uncertainties in the calculated parameter resulting from the low number of halos in this simulation). In the case of the other cosmologies we find no noticeable change of a before a redshift $z \approx 2$, followed by a mild increase from $a \approx 0.3$ to $a \approx 0.38$ at $z \approx 0$. This is also clearly visible when assessing the evolution in terms of cosmic time, as can be seen in the top right panel.

5.2 Evolution of the Faber-Jackson relation

Evolutionary trends for the Faber-Jackson relation are comparable to that seen in the Kormendy relation. No discernible trends are found in the open cosmology, while all of the other high density Universes do show a mild decrease from $b \approx 0.35$ at $z \approx 2$ to $b \approx 0.32$ at $z \approx 0$. When assessing in terms of cosmic time (center right panel), we observe a near uniform increase of b over the last 8 Gyr.

In most studied cosmologies, with the possible exception of the Λ CDMO2 cosmology, we find a marginal trend of the Fundamental Plane parameter c to decrease for $z < 2$, more or less in the past ~ 6 -7 Gyr. At earlier epochs such a trend is entirely absent. No significant evolution of the FP parameter d can be observed in Fig. 10.

5.3 Evolution of the Fundamental Plane

No significant evolution has been found for the Fundamental Plane parameters c and d (see Fig. 10, lower panels). Evolution of the Fundamental Plane mainly concerns its thickness.

In Fig. 11 we show the development of the FP thickness as a function of cosmic expansion factor $a_{exp}(t) = 1/(1+z)$ for four cosmological models, and in Figs. 13 and 12 we show the evolution of the spread of points with the FP as a function of redshift in the Λ CDMF2 model.

We see a systematic increase of FP thickness over the whole cosmic evolution in the case of the high Ω_m SCDM cosmology. While we do see a rise of the FP thickness before $a_{exp} < 0.5$ in the Λ CDMF2 and Λ CDMC2 cosmologies, after that time the increase levels off and may even flatten completely. Note, however, that these simulations do not attain sufficient halo mass resolution at higher redshifts: in

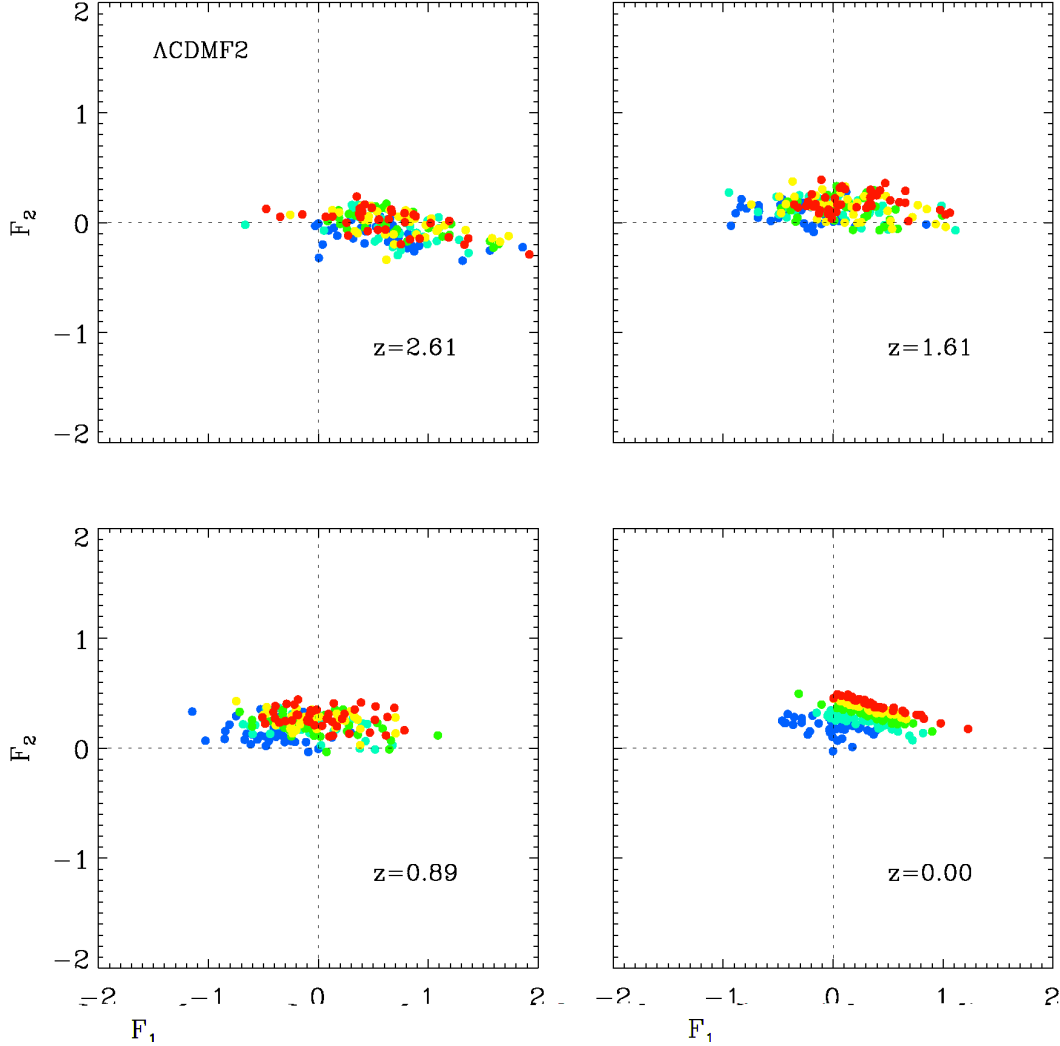


Figure 12. Shifting location of the cluster halo population within the Fundamental Plane. The depicted halo sample is the one in Λ CDMF2 cosmology, and is shown at four different redshifts: $z = 2.61$ (top left panel), $z = 1.61$ (top right panel), $z = 0.89$ (bottom left panel) and $z = 0$ (bottom right panel). The abscissa and ordinate axis are arbitrarily chosen, mutually perpendicular, axes within the FP plane defined by $(\log r_h, \mu, \log \sigma_v)$ at $z = 0$ (Eqn. 30).

these cosmologies halos still are low mass objects at these epochs. The one exceptional cosmology is that of the low Ω_m Universe Λ CDMO2. Except for a rather abrupt and sudden jump in FP thickness at $a_{exp} \sim 0.3$, there is no noticeable change at later epochs. By $a_{exp} = 0.3$ nearly all its clusters are in place and define a Fundamental Plane that does not undergo any further evolution.

In summary, the trend seems to be for initial increase of the FP thickness followed by a convergence to a nearly constant value. The epoch of convergence is later for higher values of Ω_m : while the thickness remains constant for the low Ω_m Λ CDMO2 cosmology, it involves a slow but continuous increase in the SCDM cosmology.

On the basis of their study of galaxy merging, Nipoti et al. (2003) argued that the disposition of galaxies in the Fundamental Plane is not simply a realization of the virial theorem, but contains additional information on galaxy structure and dynamics. This should be reflected in

the location of the halo population within the Fundamental Plane.

Figs. 12 and 13 show how the location of the clusters within the plane shifts as time proceeds. The color scheme is the same as for Fig. 2. Fig. 12 shows the location of the clusters in the Λ CDMF2 cosmology in the Fundamental Plane inferred for the current epoch, ie. at redshift $z = 0$,

$$\log r_h = 0.41 \mu + 1.88 \log \sigma_v + C_{fp,L} . \quad (30)$$

To locate their position within the Fundamental Plane, we use the (artificial) coordinates F_1 and F_2 of the halo points with respect to two mutually perpendicular normalized vectors in the Fundamental Plane at $z = 0$, wrt. the coordinate system defined by the FP quantities $(\log r_h, \mu, \log \sigma_v)$ (note that F_1 and F_2 do not have a specific physical significance). From the panels in the figure we see that the evolution of halos involves a gradual shift along an almost universal Fundamental Plane. It also shows that the halo population seems to evolve from a more scattered and somewhat looser one

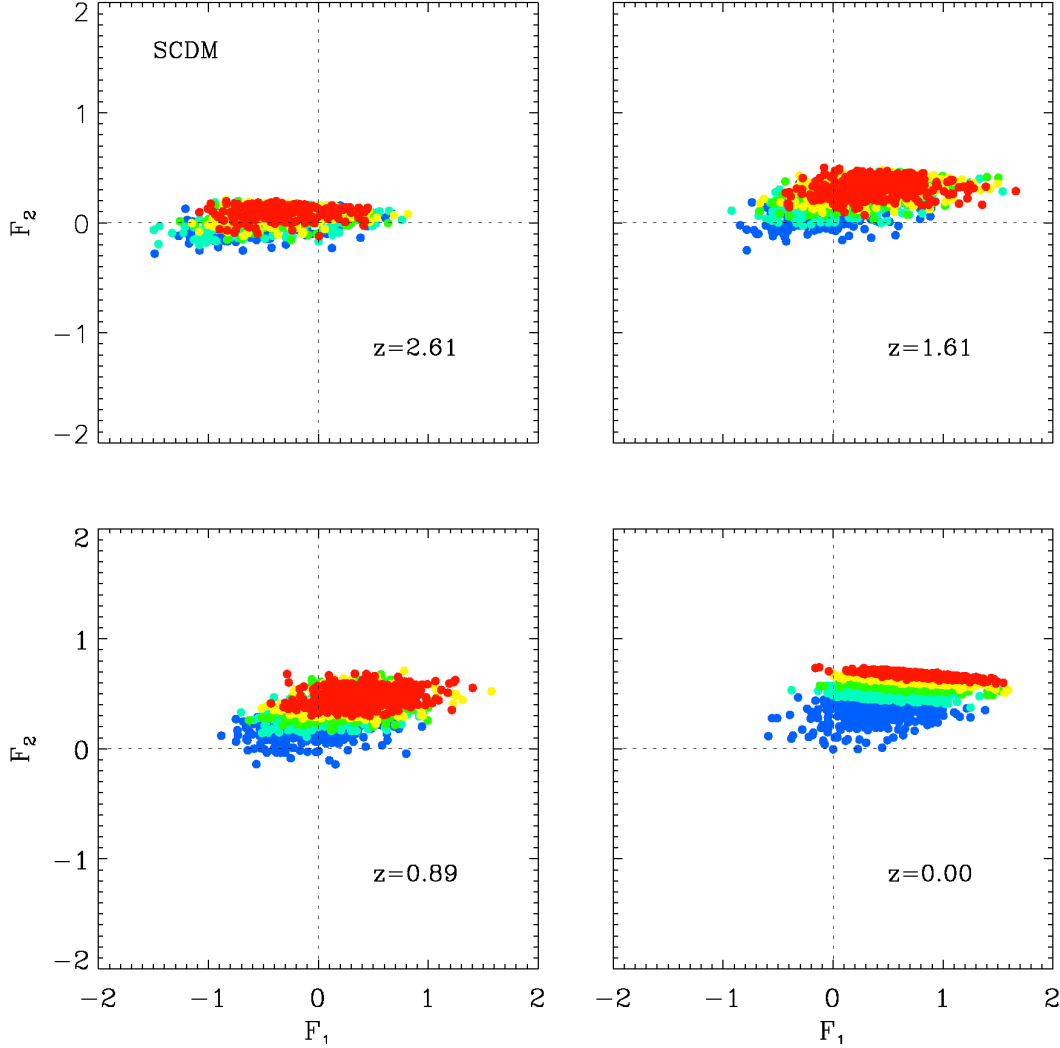


Figure 13. Shifting location of the cluster halo population within the Fundamental Plane. The depicted halo sample is the one in SCDM cosmology, and is shown at four different redshifts: $z = 2.61$ (top left panel), $z = 1.61$ (top right panel), $z = 0.89$ (bottom left panel) and $z = 0$ (bottom right panel). The abscissa and ordinate axis are arbitrarily chosen, mutually perpendicular, axes within the FP plane defined by $(\log r_h, \mu, \log \sigma_v)$ at $z = 0$ (Eqn. 31).

into a tightly elongated point cloud at the current epoch, providing interesting clues towards understanding the cluster virialization process.

In the same vein, Fig. 13 follows the changing location of clusters in the SCDM cosmology in the corresponding Fundamental Plane at $z = 0$,

$$\log r_h = 0.37 \mu + 1.78 \log \sigma_v + C_{fp,S}. \quad (31)$$

Similar to the Λ CDMF2 cosmology, we find that the cluster point cloud appears to assume a clearer mass stratification as time proceeds. While the population of clusters in the SCDM cosmology also appears to shift its location along the Fundamental Plane as it evolves, we do not find a trend towards a more tightly point cloud that we see in the LCDMF2 cosmology. We will investigate these evolutionary trends in more detail in an upcoming study, we have found indications for a possible influence of the different cluster halo merging histories in SCDM and Λ CDMF2 in explain-

ing the different behaviour of the cluster point clouds in the Fundamental Plane.

6 MERGING AND ACCRETION DEPENDENCE

Figures Fig. 10 and Fig. 11 show that the evolution of the parameters defining these relationships is very erratic. This testifies to the fact that in hierarchical structure formation scenarios the formation and evolution of halos is hardly a quiescent and steadily progressing affair. Rather, halos grow in mass by steady accretion of matter from its surrounding as well through the merging with massive peers. Even the accretion is not a continuous and spherically symmetric process: most matter flows in in a strongly anisotropic fashion through filamentary extensions into the neighboring large scale matter distribution. As a result, we can expect that many halos will not have settled into a perfect virial state.

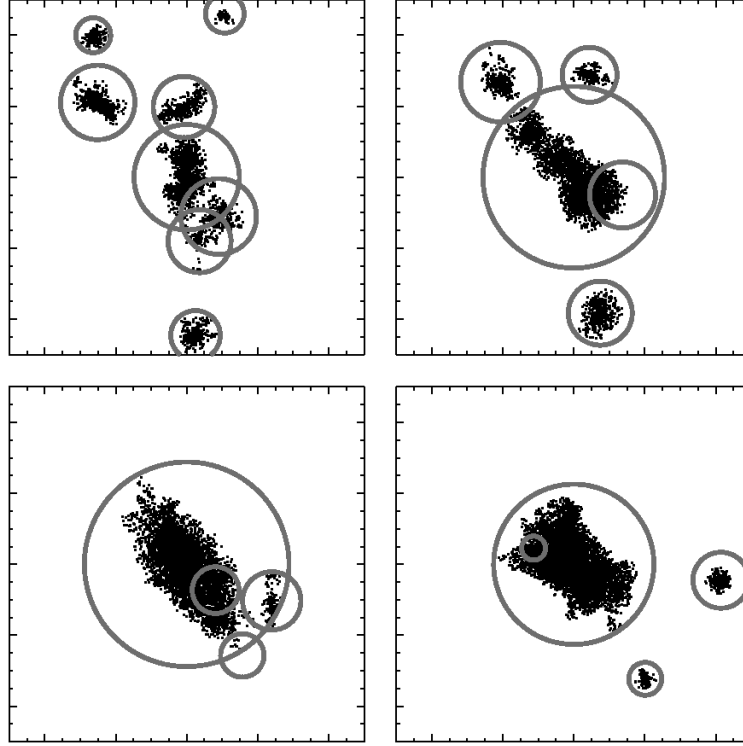
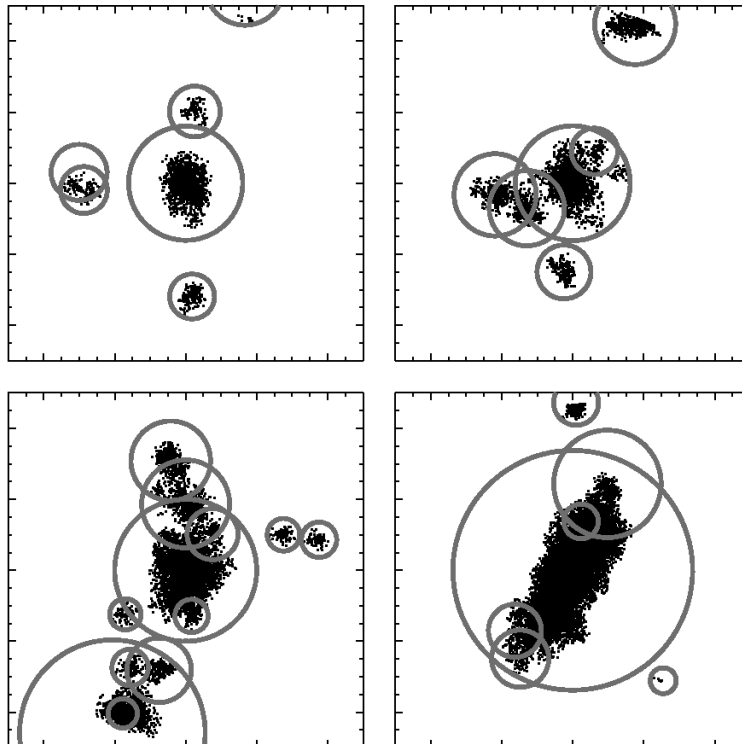


Figure 14. Accreting vs. Merging Halo Evolution: the evolution of two different halos in the Λ CDMF2 cosmology. Each panel concerns a $5h^{-1}$ Mpc comoving size box centered on the core of the halo. The sequence runs from $z = 2.61$ (top left panel), via $z = 1.61$ (top right panel), to $z = 0.89$ (bottom left panel) and finally the present epoch $z = 0$ (bottom right panel). The circles indicate the location of HOP identified halos, with the size of the circle being proportional to the (virial) radius of the halo (overlapping circles are due to the projection of the corresponding spheres). Top four panels: a quiescently evolving accreting halo. Bottom four panels: a strongly hierarchically evolving merging halo.



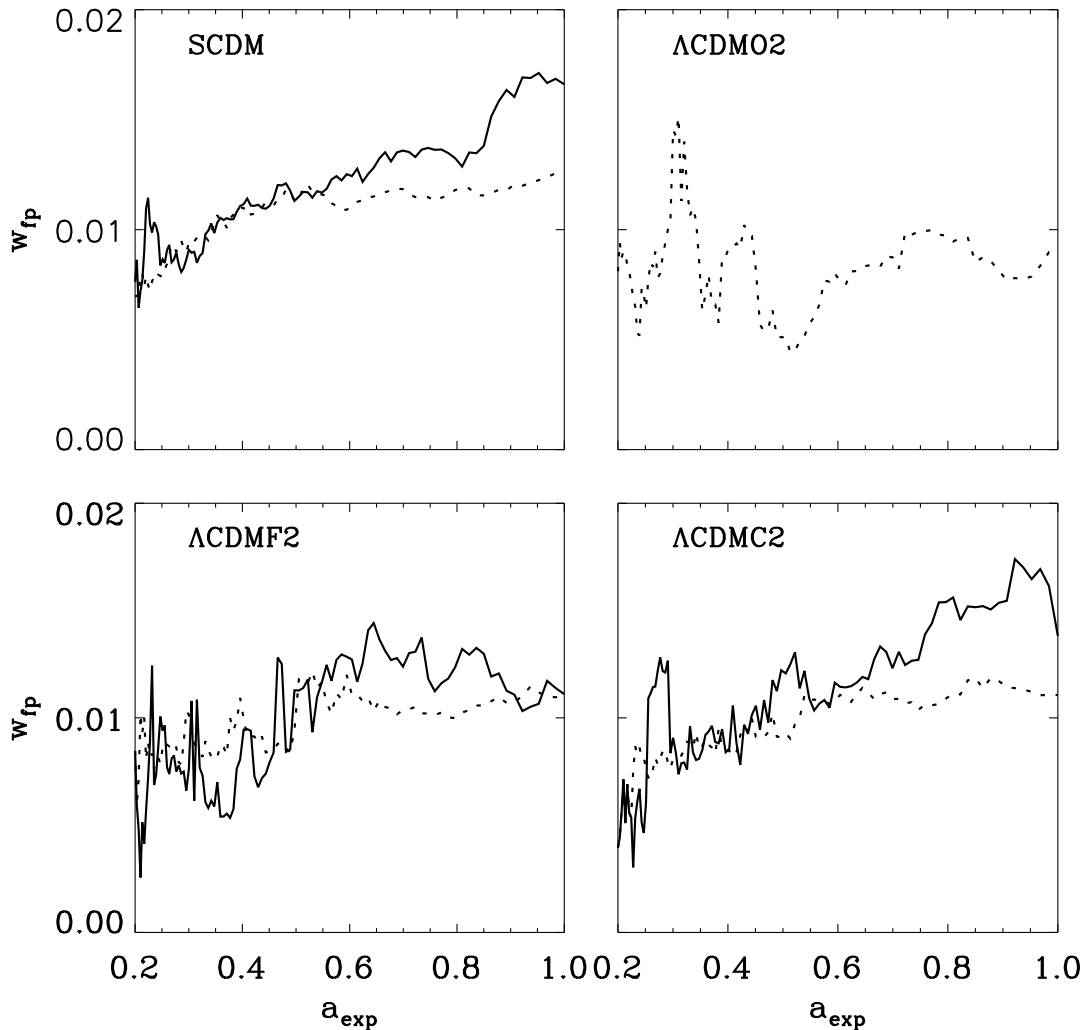


Figure 15. Thickness of the Fundamental Plane when considering accretion (dotted lines) or mergers (solid lines).

This will certainly be the case for halos that recently suffered a major merger with one or more neighboring clumps.

The detailed accretion and merging history is a function of the underlying cosmology. Low density cosmologies or cosmologies with a high cosmological constant will have frozen their structure formation at early epochs. The halos that had formed by the time of that transition will have had ample time to settle into a perfect virialized object. Also, there is a dependence on the power spectrum of the corresponding structure formation scenario. Power spectra with a slope $n < -1.5$ (at cluster scales) will imply a more homologous collapse of the cluster sized clumps, less marked by an incessant bombardment by smaller clumps. It may be clear that a more violent life history of a halo will usually be reflected in a substantial deviation from a perfect virial state.

In order to investigate the implications of a difference in accretion or merging history of halos, we have split the samples of cluster halos in each of our cosmologies into a *merging sample* and a *accretion sample*. Possible differences in their virial state should be reflected in the quality of the

scaling relations, in particular that of the thickness of the Fundamental Plane.

The *merger sample* consists of those halos that suffered a merger with another halo that contained at least 30% of its mass. Fig. 14 shows two examples of halos in the Λ CDMF2 cosmology. The top sequence of 4 panels shows the evolution of a quiescently evolving *accretion halo*, by means of the particle distribution in a $5h^{-1}$ Mpc box (comoving size) around the cluster core, at $z=2.61$, $z=1.61$, $z=0.89$ and $z=0.00$. The circles indicate the location of the HOP identified halos, with the size of the circle proportional to the radius of the halo (note that the overlap of circles is due to projection of the halo spheres). The lower group of 4 panels shows the particle distribution at the same redshifts for a halo belonging to the *merging sample*. Its gradual hierarchical buildup is directly visible as the continuous infall of clumps at each timestep.

In Fig. 15 we show the evolution of the thickness of the Fundamental Plane for each of the two samples in the four indicated cosmologies. Note that our simulations do not have sufficient resolution for reconstructing the precise merging or

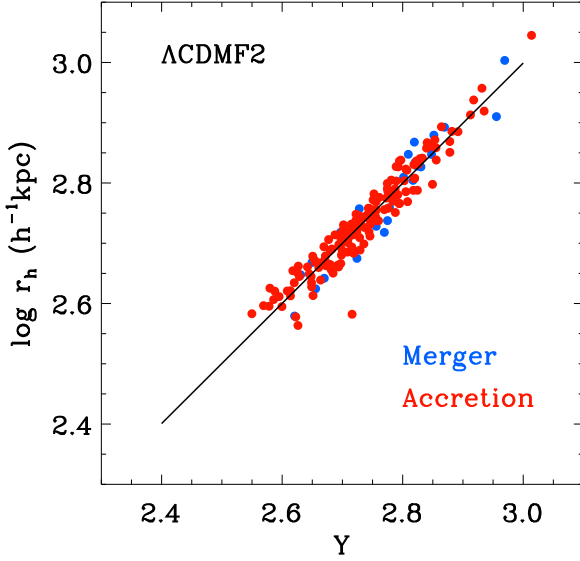


Figure 16. Comparison between the Fundamental Plane in the Λ CDMF2 cosmology for clusters that underwent a major merger (blue dots) and clusters that followed a more quiescent accretion history (red dots). The plot depicts the relation between harmonic radius r_h and the quantity $Y = c\mu + d\log\sigma + C_{fp}$, in which c and d are the FP scaling parameters.

accretion history before $a_{exp} = 0.3 - 0.4$, so that we may not draw conclusions on the rise of the FP thickness up to that epoch. Also, in the case of the Λ CDMO2 scenario we do not have enough cluster halos to be able to detect any systematic differences between the merging and accreting halos.

In the more recent history we do find some significant differences between merging and accretion-only halos in various cosmologies, in particular the ones with a high Ω_m . There does not seem to be a systematic difference between these groups in the Λ CDMF2 cosmology. The total absence of any difference between the Fundamental Plane of merging and accreting cluster halos at present (Fig. 16), is the outcome of an evolutionary history without any significant differences between the two subsamples (Fig. 15, lower left-hand panel).

The story is quite different for the Λ CDMC2 and SCDM cosmology. While the cluster halos that undergo a major merger do reveal a constantly growing FP thickness, their accretion-only clusters do not display such a systematic increase. Instead, their FP thickness remains lower and levels off. In other words, accretion halos (dotted lines) do on average display a tighter FP relation. This is particularly true at the current epoch. Apparently, the absence of violent mass gain in the case of accretion halos implies that they have more time to relax and virialize. This, in turn, is reflected in a thickness of the Fundamental Plane which does not evolve any further. Interestingly, it is also reflected in the radii of the halos (Fig. 17): while the harmonic radius and half-mass radius of accreting cluster halos are mostly in accordance with each other, though with a larger spread than in the case of Λ CDMF2 clusters (lower panel), the SCDM halos that underwent major mergers do appear to be responsible for the substantial differences between the harmonic and

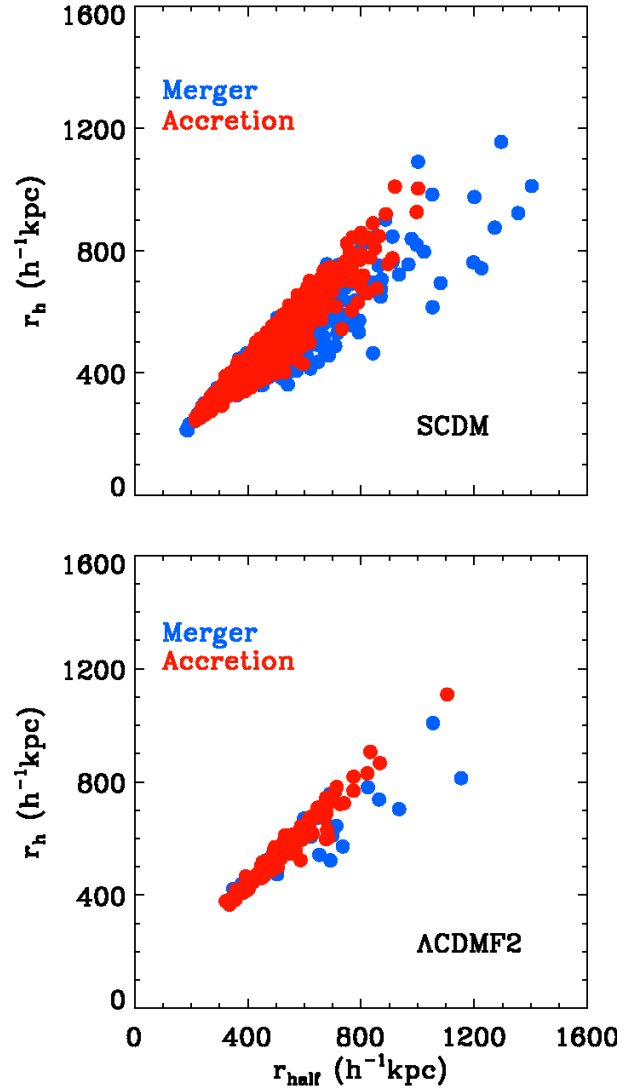


Figure 17. Comparison between the mean harmonic radius and the half-mass radius of the halos in the SCDM (top) and Λ CDMF2 (bottom) scenarios. The cluster samples are split into the clusters that underwent a major merger (blue dots) and the ones that accreted matter in a more quiescent fashion (red dots). See text for further explanation.

half-mass radii that we see in Fig. 2. From this we conclude that the accretion history is a major factor in determining the character of the Fundamental Plane, via the impact of mergers on the mass distribution within halos and hence their radii. We discuss this in more detail in the next section 7.

The implications of this finding might be far-reaching. Given the remarkable robustness and stability of the Fundamental Plane, any deviation of individual clusters from the FP may be a direct reflection of its recent dynamical evolution. This would be true if the thickness of the plane would be entirely due to the merger history of the clusters. It is certainly a viable implication of our conclusion that the Fundamental Plane's definition – the average plane of

a large sample of clusters – is nearly unassailable while we find strong fluctuations and deviations from the average FP in small samples of actively evolving clusters.

In practice, it might mean that one could take samples of clusters in different redshift bands and reliably average them in each band to use the resulting Fundamental Plane to study redshift evolution of observed samples. It would also mean that within each redshift band you know which ones have had active lives.

7 RECONCILING THE SIMULATIONS WITH THE VIRIAL THEOREM

7.1 The Virial Theorem

The Fundamental Plane is a direct reflection of the virial theorem which, under particular assumptions, relates the averaged velocity dispersion and radius of a system directly to its mass. All “virialised” objects will lie on a plane defined in the space of those three variables. There is not even any freedom in the parameters for that plane: its slope and location are fixed for all virialised objects.

There are complications when assigning data to a Fundamental Plane. Firstly, in its simplest form, the virial theorem assumes that the virialised objects are isolated spherical systems and, importantly, that they are stationary. The systems we study are not spherical and they are certainly not stationary: they are generally in a state of dynamical evolution. The possible exception to this might be the largest most isolated systems. Secondly, observed data does not have direct knowledge of the system mass except through interpreting the light that is observed. The universality of the Fundamental Plane allows us to turn the problem around and determine the dependence of light on mass in order that systems should fit on the Fundamental Plane. The simplest approach to this is to assume that the mass to light ratio in the observed waveband is directly related to mass.

There are further issues. For example, what do we mean when we refer to “averages” of quantities? Using a different averaging process yields a different Fundamental Plane. There is also the fact that astrophysical systems are observed only in projection.

Having said that, we can express the Virial Theorem in terms of the variable we have used here to describe the Fundamental Plane. With the notation that a virialised system of mass M has a velocity dispersion V , half mass radius r_{half} and harmonic radius r_h we have, up to normalising constants:

$$V^2 = \frac{M}{r_h^2}, \quad \Sigma = \frac{M}{r_{half}^2} \quad (32)$$

where Σ is the projected (surface) mass density. Eliminating M from these and taking logs yields an expression for the Fundamental Plane:

$$\log r_h = \left(\frac{r_h}{r_{half}} \right) + 2 \log V + 0.4\mu \quad (33)$$

where we have transformed the surface mass density Σ into logarithmic astro-units via

$$\mu = -2.5 \log \Sigma \quad (34)$$

We have explicitly written equation (33) in such a way as

to expose the different roles of harmonic and half-mass (geometric) radii. The relationship between these radii in our models is illustrated in Fig. 2 and in Fig. 17, the latter differentiating between merging and quiescently accreting halos.

7.2 Renormalising the FP Simulations

It is important to understand why the coefficients of the model Fundamental Plane might differ from the expectations based on the use of the virial theorem. Luminosity is not involved here so we cannot appeal to a varying mass-to-light ratio. Moreover, the model Fundamental Plane is well defined and so we cannot say that this is merely a question of fitting.

There are at least two possible sources for this systematic difference between the model and the virial theorem. The first is to blame the HOP technique and assert that it systematically underestimates the cluster masses. The second is to say that the internal cluster properties (like velocity distribution) vary systematically with mass and so the normalisation of the virial plane is mass dependent.

Either way, we shall model in a mass dependency and consider this in relation to the HOP technique. The process for the variable virial normalisation is analogous.

The samples of clusters derived from these simulations are all based on the HOP technique. There may well be a systematic bias in the assignment of particles to clusters (see section 2.1). As a consequence, the radii and velocity dispersion derived for a HOP selected cluster will also be biased. Clearly the bias will be more significant for smaller systems.

In this subsection we seek to account for systemic effects of using HOP for identifying cluster membership, and derive a renormalisation procedure taking account of this and matching the dataset to the expected virial theorem Fundamental Plane (equation 33).

The easiest way to model this bias is to assume that the model-based estimate (biased) for the mass, M , is related to the actual mass \mathcal{M} by a simple scaling relationship

$$\frac{\mathcal{M}}{M} \propto \mathcal{M}^{\frac{\alpha}{1+\alpha}} \quad (35)$$

for some exponent α . The virial expression for the mass then becomes

$$V^2 = \left(\frac{\mathcal{M}}{M} \right) \frac{M}{r_h^2} = M^{-\alpha} \frac{M}{r_h^2} \quad (36)$$

where the right hand side now refers to quantities derived from the model. We can eliminate M from this in terms of the model surface mass density $\Sigma = M/r_h^2$ to give

$$r_h = \left(\frac{r_h}{r_{half}} \right)^{\frac{2}{1+\alpha}} V^{2(\frac{1-\alpha}{1+\alpha})} \Sigma^{-\frac{1}{1+\alpha}} \quad (37)$$

Taking logs and using $\mu = -2.5 \log \Sigma$ finally yields

$$\log r_h = \frac{2}{1+\alpha} \log \frac{r_h}{r_{half}} + 2 \frac{1-\alpha}{1+\alpha} \log V - \frac{0.4}{1+\alpha} \mu \quad (38)$$

which is the expression for the Fundamental Plane in terms of the (biased) model derived quantities. This should be compared with equation (33): we see how the bias modelled by α affects the position and slope of the virial Fundamental Plane.

Model	d	α	c	c(model)
SCDM	1.78 ± 0.01	0.058 ± 0.003	0.38	0.37 ± 0.031
LCMDF1	1.69 ± 0.084	0.084 ± 0.024	0.37	0.38 ± 0.016
LCDMF2	1.88 ± 0.04	0.031 ± 0.011	0.39	0.41 ± 0.011
LCDMF3	1.81 ± 0.02	0.050 ± 0.014	0.38	0.38 ± 0.056
OCDM01	1.60 ± 0.083	0.111 ± 0.024	0.36	0.35 ± 0.017

Table 5. Fitting biased models to ideal virial Fundamental Plane. The parameter α emulates the limitations of the HOP group finder.

The procedure now, for each simulation, is to select a value of α that makes the coefficient of $\log V$ in equation (38) equal to the virial value 2. That α then allows a calculation of the coefficient of μ that can be compared with the value derived from the simulation. The results for a selection of models is shown in Table 5.

The conclusion to be drawn from this is that, for each model, there is indeed a value of the α parameter that reproduces the Fundamental Plane fits for the models.

7.3 Observed cluster FP

The best available data set is the ENACS data of (Adami et al. 1998). Equation (17) describing that Fundamental Plane, in the current notation, reduces to

$$\log R_e = (0.49 \pm 0.05)\mu + (1.12 \pm 0.11) \log \sigma_v \quad (39)$$

There is considerable uncertainty in this relationship: the coefficient of $\log \sigma$ is quite far from the ideal 2.0 and the coefficient of μ is higher than the nominal 0.4.

The usual way to reconcile this with the virial Fundamental Plane is to argue that the mass to light ratio of the cluster sample is mass dependent:

$$\frac{M}{L} \propto M^\beta \quad (40)$$

Using an argument that parallels the derivation of equation (38), the Fundamental Plane expressed in terms of velocity and surface mass density is

$$\log r_h = \frac{2}{1+\beta} \log \frac{r_h}{r_{half}} + 2 \frac{1-\beta}{1+\beta} \log V - \frac{0.4}{1+\beta} \mu \quad (41)$$

The data give $\beta = 0.28 \pm 0.19$ which gives rise to $c = 0.31 \pm 0.02$, a long way from the data-derived 0.49. It is clearly not possible to reconcile the ENACS data with the virial theorem Fundamental Plane, let alone the numerical simulations.

8 CONCLUSIONS AND DISCUSSION

We have studied three structural scaling relations of galaxy clusters in thirteen cosmological models. These relations are the Kormendy relation, the Faber-Jackson relation and the Fundamental Plane. Their validity and behavior in the different cosmological models should provide information on the general virial status of the cluster halo population. The cosmological models that we studied involved a set of open, flat and closed Universes with a range of matter density parameter Ω_m and cosmological constant Ω_Λ .

The cluster samples are obtained from a set of N -body simulations in each of the cosmologies. These simulations concerns a box of $200h^{-1}\text{Mpc}$ with 256^3 dark matter particles. The initial conditions were set up such that the phases of the Fourier components of the primordial density field are the same for all simulations. In this way, we have simulations of a comparable morphological character: the same objects can be recognized in each of the different simulations (be it at a different stage of development).

After running the simulations from $z = 4$ to the current epoch using the GADGET2 code, we used HOP to identify the cluster halos. We investigated whether each halo population obeyed a mass-radius relation akin to the Kormendy relation, a mass-velocity dispersion relation similar to the Faber-Jackson relation and a two parameter family between mass, radius and velocity dispersion that resembles a Fundamental Plane relation. We studied the dependence of the obtained scaling parameters as a function of the underlying cosmology and investigated their evolution in time.

Our results can be summarized as follows:

- In each cosmological model we do recover Kormendy, Faber-Jackson and Fundamental Plane relations for the population of cluster halos. This is a strong indication that the halos are in a virialized state, as expected in hierarchical clustering scenarios.

- There are significant differences between the measured parameters of the various scaling relations and those seen in the observational data. Our fit for the FP in the LCMDF2 model is

$$\log r_h = 0.41\mu + 1.86 \log \sigma + \text{const.} \quad (42)$$

This can be reconciled with the expectation from the virial theorem, but not with the ENACS Fundamental Plane.

- We do not find any significant dependence of the parameters a and b of the Kormendy and Faber-Jackson relations on the value of Ω_m . There is also no indication for any influence of Ω_Λ on the scaling relations.

- While the FP parameters c and d are not dependent on Ω_m and Ω_Λ , there is a slight suggestion that the Fundamental Plane would have a lower thickness for low $\Omega_m \sim 0.1$ cosmologies.

- With the exception of low Ω_m Universes, we find a mild increase of the Kormendy parameter a and a mild decrease of the Faber-Jackson parameter b from $z = 1$ to the present epoch. From $z = 4$ to $z = 1$ we did not find any discernable evolution.

- While the Fundamental Plane parameters c and d do in general not show a significant evolution, the higher Ω_m cosmologies do involve a slight decrease of FP parameter d during most recent epochs ($z < 2$).

- The thickness of the Fundamental Plane does evolve significantly, with an initial increase followed by a convergence to a more or less constant value. The convergence epoch is later for higher density cosmologies. This probably reflects the gradually virializing tendency of the cluster population.

- Given our expectation that there is a difference in virial state between quiescently accreting clusters and those experiencing massive mergers, we have investigated the evolution of the Fundamental Plane thickness for samples of merging clusters and samples of accreting clusters. We find that accreting clusters at recent epochs do appear to be bet-

ter virialized than the merging population and that the FP thickness is smaller in the former.

- We find that for all investigated cosmologies the Fundamental Plane is remarkably stable, despite the enormous evolution of the individual systems. The only significant evolution, that of its thickness, might be due in a large part to the importance of merging of individual systems.

- If indeed the thickness of the Fundamental Plane might be entirely due to the merger history of the cluster halos, the distance of an individual cluster to the Fundamental Plane would be a direct reflection of the cluster history.

- We see direct evidence that major mergers have effected the relationship between the galaxy haloes in the cluster in that the relationship between the half-mass and harmonic radii is disturbed. Nonetheless, the evidence from the models tells us that this does not affect the slope of the Fundamental Plane: clusters that have undergone major mergers lie in the same place as those that have grown by steady accretion.

Finally, what is desperately needed is better data on the cluster fundamental plane. We might speculate that the distance of a cluster from the plane defined by the data somehow reflects the evolution of the cluster, but we will not get evidence for the hypotheses derived from numerical experiment until there is more high quality data.

ACKNOWLEDGEMENTS

P.A. gratefully acknowledges support by NOVA. RvdW is grateful for the support and great hospitality of KIAS during the completion of this manuscript. In addition, BJ gratefully acknowledges the hospitality of the Kapteyn Astronomical Institute in Groningen, and to his collaborators for their remarkable patience in getting various parts of this paper completed.

REFERENCES

- Adami C., Mazure A., Biviano A., Katgert P., Rhee G., 1998, *A&A*, 331, 493
- Bernardi M., et al., 2003, *AJ*, 125, 1866
- Bertin G., Ciotti L., Del Principe M., 2002, *A&A*, 386, 149
- Binney J., Merrifield M., 1998, *Galactic Astronomy* / James Binney and Michael Merrifield. Princeton, NJ : Princeton University Press, 1998.
- Bolton A. S., Burles S., Treu T., Koopmans L. V. E., Moustakas L. A., 2007, *ApJL*, 665, L105
- Cappellari M., et al. 2006, *MNRAS*, 366, 1126
- Djorgovski S., Davis M., 1987, *ApJ*, 313, 59
- Dressler A., Lynden-Bell D., Burstein D., Davies R. L., Faber S. M., Terlevich R., Wegner G., 1987, *ApJ*, 313, 42
- Eisenstein D. J., Hut P., 1998, *ApJ*, 498, 137
- Faber S. M., Jackson R. E., 1976, *Apj*, 204, 668
- Faber S. M., 1987, *Nearly Normal Galaxies. From the Planck Time to the Present*, Proceedings of the Eighth Santa Cruz Summer Workshop in Astronomy and Astrophysics, Santa Cruz, CA, July 21-Aug. 1, 1986
- González-García A. C., van Albada T. S., 2003, *MNRAS*, 342, L36
- González-García A. C., 2003, Ph.D. Thesis, University of Groningen, The Netherlands
- Helmi A., 2000, Ph.D. Thesis, Leiden Observatory, Leiden University, The Netherlands
- Helmi A., White S. D. M., 1999, *MNRAS*, 307, 495
- Jørgensen I., Franx M., Kjaergaard P., 1995, *MNRAS*, 276, 1341
- Jørgensen I., Franx M., Kjaergaard P., 1996, *MNRAS*, 280, 167
- Kormendy J., 1977, *ApJ*, 218, 333
- Kormendy J., 1987, *Nearly Normal Galaxies. From the Planck Time to the Present*, Proceedings of the Eighth Santa Cruz Summer Workshop in Astronomy and Astrophysics
- La Barbera F., Busarello G., Merluzzi P., Massarotti M., Capaccioli M., 2003, *ApJ*, 595, 127
- Lahav O., Lilje P. B., Primack J. R., Rees M. J., 1991, *MNRAS*, 251, 128
- Lanzoni B., Ciotti L., Cappi A., Tormen G., Zamorani G., 2004, *ApJ*, 600, 640
- Marmo C., Fasano G., Pignatelli E., Poggianti B., Bettoni D., Halliday C., Varela J., Moles M., Kjaergaard P., Couch W., Dressler A., 2004, in *Outskirts of Galaxy Clusters: Intense Life in the Suburbs*. Edited by Antonaldo Diaferio, IAU Colloquium No.195, p.242-244
- Nigoche-Netro A., Ruelas-Mayorga A., Franco-Balderas A., 2009, *MNRAS*, 392, 1060
- Nipoti C., Londrillo P., Ciotti L., 2003, *MNRAS*, 342, 501
- D'Onofrio M., Fasano G., Varela J., Bettoni D., Moles M., Kjaergaard P., Pignatelli E., Poggianti B., Dressler A., Cava A., Fritz J., Couch W. J., Omizzolo A., 2008 *ApJ*, 685, 875
- Perlmutter S., et al., 1999, *ApJ*, 517, 565
- Riess A. G., et al., 1998, *AJ*, 116, 1009
- Robertson B., Cox T. J., Hernquist L., Franx M., Hopkins P. F., Martini P., Springel, V. 2006, *ApJ*, 641, 21
- Schaeffer R., Maurogordato S., Cappi A., Bernardeau F., 1993, *MNRAS*, 263, L21
- Spergel D. N., et al., 2007, *ApJS*, 170, 377
- Spergel D. N., Verde L., Peiris H. V., et al. 2003, *ApJS*, 148, 175
- Springel V., 2005, *MNRAS*, 364, 1105
- Tully R. B., Fisher J. R., 1977, *A&A*, 54, 661
- van Dokkum P. G., Franx M., 1996, *MNRAS*, 281, 985

This paper has been typeset from a \TeX / \LaTeX file prepared by the author.